Available online at www.sciencedirect.com
ScienceDirect
Journal of Sound and Vibration 317 (2008) 800–840
JOURNAL OF SOUND AND VIBRATION
www.elsevier.com/locate/jsvi

Vibrational power flow models for transversely vibrating finite Mindlin plate

Young-Ho Park, Suk-Yoon Hong*

Department of Naval Architecture and Ocean Engineering, Seoul National University, San 56-1 Sillim-dong, Kwanak-gu, Seoul, 151-742, Republic of Korea

Received 28 March 2007; received in revised form 20 December 2007; accepted 30 March 2008
Handling Editor: L.G. Tham
Available online 16 June 2008

Abstract

In this paper, power flow models were developed to analyze transversely vibrating finite Mindlin plate considering the effects of shear distortion and rotatory inertia, which are very important at high frequencies. The energy governing equations for far-field propagating out-of-plane waves in the Mindlin plate were newly derived by using the classical displacement solutions for out-of-plane motions in the Mindlin plate. The derived energy governing equations are composed of the energetics of three kinds of far-field propagating waves. Below the critical frequency, the energy governing equation for only one kind of far-field propagating wave, which is analogous to that for flexural wave in the Kirchhoff plate, is obtained. On the other hand, above the critical frequency, the energy governing equations for all three kinds of far-field propagating waves are derived. The developed power flow models are in the general forms incorporating not only the Mindlin plate theory but also the Kirchhoff plate theory. To verify the validity and accuracy of the derived models, numerical analyses are performed for the case where the finite Mindlin plates are excited by a harmonic point force, and the spatial distributions and levels of energy density and intensity obtained by the developed power flow solutions for the Mindlin plate are compared with those obtained by the classical displacement solutions for the Mindlin plate, the traditional power flow solutions, and the classical displacement solutions for the Kirchhoff plate for various excitation frequencies and hysteretic damping factors.

1. Introduction

The remarkable development of automotive, electronic and aerospace industries has been raising the interest of high-frequency noise and vibration over the last decades. Consequently, suitable high-frequency noise and vibration prediction tools for various built-up structures are required that can assist in identification of structure-borne noise paths and potential hot spots (i.e. components with relatively high vibrational energy). However, there is currently no one suitable method for predicting structure-borne noise of built-up structures, such as automotive vehicles, household electric appliances and aircrafts, throughout the entire audible frequency range (i.e. 20–20,000 Hz).

*Corresponding author. Tel.: +82 2 880 8757; fax: +82 2 888 9298.
E-mail address: syh@snu.ac.kr (S.-Y. Hong).

0022-460X/$ - see front matter © 2008 Elsevier Ltd. All rights reserved.
doi:10.1016/j.jsv.2008.03.049

At low frequencies, the deterministic approach based on traditional displacement solutions (i.e. modal solutions) has been effectively used for prediction of structure-borne noise (vibration) of built-up structures. Because of the relative large size of the wavelengths with respect to the size of each component in this frequency region, small uncertainties in the properties of the short members will not impact their distinctly resonant behavior. Therefore, the conventional finite element analysis (FEA) and boundary element analysis (BEA) that apply numerical techniques to equations of dynamic motion have become firmly established as the most widely used analytical vibration and noise prediction tools for practical engineers.

At high frequencies, the deterministic approach based on the analytical and asymptotic methods such as the geometrical theory of diffraction (GTD), ray method and W.K.B. method have been proposed for prediction of acoustic and vibrational responses since early times [1–5]. Though these deterministic methods provide approximate expressions of the solution under high-frequency approximation, those are potentially computationally expensive and time consuming to develop and check out analytical models for built-up structures. In addition, there are other reasons that the deterministic approach is not practical for prediction of structure-borne noise at high frequencies. The vibrational behavior of a structure at high frequencies becomes increasingly dependent on fine structural details such as structural joints and boundaries, which cannot be mathematically represented with sufficient accuracy in these frequencies range [6,7]. Also, high-frequency acoustic and vibrational responses of nominally identical structures are observed to be different due to fabrication tolerances allowed during manufacturing processes in mechanical industries [8,9]. Therefore, because the large statistical variation observed at high frequencies is typical in practical engineering, the usefulness of deterministic methods in the capacity of structure-borne noise prediction tool is limited.

As the alternative to deterministic approaches at high frequencies, the statistical approach was proposed to predict modal- and frequency-averaged dynamic behavior of a structure. The statistical approach allows for a much simpler description and measurement of the system, whether the field is described by modes or wave [10]. However, the most obvious disadvantage of statistical approaches is that they give statistical answers, which are always subject to some uncertainty. These characteristics of statistical approaches cause the researchers concerned to develop theories of the variance, mean, and the confidence for prediction intervals [11,12].

Statistical energy analysis (SEA), the representative analytical method of statistical approaches, is used to effectively predict the space- and frequency-averaged behavior of built-up structures at high frequencies where the modal density of structures is high. However, by SEA approximation, lumped dynamic characteristics are used to represent continuous linear systems. Therefore, SEA can predict only a single acoustic or vibrational energy value for each subsystem of a built-up structure. Additionally, because the power balance equation of SEA is linear algebraic equation, the finite element and boundary element methods, which are very effective numerical techniques for solving differential equations with arbitrary boundary conditions, cannot be applied to SEA. Consequently, the FEA/BEA database model, which generally takes most of total analysis time at low frequencies, cannot be used directly for SEA modeling [13].

Although SEA is one of statistical methods that are reasonable prediction tools at high frequencies, the weaknesses of SEA have motivated researchers to investigate several alternative structure-borne sound prediction tools that can be applicable to a numerical implementation such as finite element method and boundary element method, and predict the spatial variation of vibrational responses in built-up structures. Power flow analysis (PFA) is the representative product of such investigations. PFA can predict locally space- and frequency-averaged vibrational behavior of arbitrary built-up structures by virtue of the governing differential equation. The heat conduction type governing differential equation of PFA describes the state of far-field vibrational energy, and makes it possible to effectively predict the far-field vibrational behavior of arbitrary built-up structures with coarse mesh compared to conventional FEA using a numerical implementation such as finite element method. PFA was first introduced by Belov et al. [14]. Nefske and Sung implemented a finite element formulation of the vibrational energy equation to predict the vibrational response of the Euler–Bernoulli beam [15]. Rods and Euler–Bernoulli beams were further studied by Wohlever and Bernhard [16,17]. Bouthier and Bernhard extended the work of Wohlever et al. [18–21] to analyze the energetics of a membrane, Kirchhoff plate and acoustic cavity. Park et al [22]. developed power flow models for in-plane waves in thin plates. To derive the heat conduction type governing differential equations of PFA based on plane wave components, two approximations are generally used. One is the local space-average over

half a wavelength to remove the spatially harmonic component and the other is the exclusion of near-field components which are dominant only near the discontinuities. Therefore, the total vibrational energy density in PFA is approximated by the smooth far-field energy density and not the harmonic far-field energy density.

Although PFA is the more advanced vibrational prediction tool compared to SEA, the effort to improve the theory of PFA has persisted. Langley showed that standard two-dimensional governing differential equation of PFA based on plane wave components would be valid only for the structure having highly reverberant wave field [23,24]. Consequently, Kim et al. suggested a modified governing differential equation of PFA in cylindrical coordinate system for predicting the energy distribution in non-diffuse field [25]. Although the wave field is effectively diffused on a rectangular plate in which numerous reflections of waves from the boundaries occur, and can be approximated by the field of randomly oriented plane waves, the wave field is not diffused on an infinite or circular plate which consists of cylindrical waves concentric with the driving point. Therefore, the standard energy governing equation of PFA is only applicable to the reverberant energy field of energy, and the modified energy governing equation of PFA is only applicable to the direct energy field. Smith suggested a hybrid energy method in which the total vibration field is divided into a direct field and a reverberant field [26]. It can predict the energy distribution over the whole plate that is equivalent to the result by classical displacement solution in a point-excited plate regardless of wave field's diffuseness. Le Bot expanded the energy governing equation of PFA into modified differential equations for each of the plane cylindrical and spherical wave fields for a general three-dimensional vibroacoustic problems [27,28]. Additionally, Lase and Jezequel suggested a General Energy Method (GEM) considering both active and reactive energy components for predicting exact energy distribution in one-dimensional structures without approximation from the deterministic point of view [29,30]. However, GEM has the weaknesses that it is more computationally intensive than the classical displacement solution, and is not easy to be applied to higher-order structures such as thin plates.

Until now, most researches on PFA have been restricted to the analysis of fundamental structures such as rods, Euler–Bernoulli beams, membranes and Kirchhoff plates. Although PFA is a more suitable method for high-frequency range than for low-frequency range, the existing traditional power flow models for out-of-plane waves cannot consider very important phenomena in high-frequency range, namely the effects of shear distortion and rotatory inertia. Therefore, power flow models by advanced theories such as the Timoshenko beam theory and the Mindlin plate theory that account for these effects must be developed to improve the prediction of vibrational behavior of a structure in the medium-to-high frequency ranges. In relation to this work, Park et al. developed the power flow models for coupled Timoshenko beams. We newly derived the energy governing equations for two kinds of flexural waves in the Timoshenko beam and extended the application of the derived energy governing equations to coupled beam structures with general beam joints through the wave transmission analyses [31,32]. However, the power flow model for out-of-plane waves in the Mindlin plate has never been developed [33].

In this paper, the energy governing equations for three kinds of far-field propagating out-of-plane waves in the Mindlin plate are derived. The derived energy governing equations for far-field out-of-plane waves is very useful to predict the reverberant portion of the vibrational energy in a finite Mindlin plate. When the excitation frequency is lower than the critical frequency determined by material properties and thickness of the plate, the energy governing equation for only the bending dominant flexural wave, which is analogous to that for the flexural wave in the Kirchhoff plate, is obtained. On the other hand, when the excitation frequency is higher than the critical frequency, energy governing equations for all three kinds of far-field propagating out-of-plane waves are obtained. Finally, to verify the accuracy and validity of the developed power flow models, the developed power flow solutions and the classical solutions for out-of-plane motions in the Mindlin plate are compared for several different conditions, and the classical and the developed PFA results for the Mindlin plate are also compared with those for the Kirchhoff plate.

2. Mindlin plate theory

The Mindlin plate theory contains two rotations as field variables in addition to the transverse displacement and can consider the effects of rotatory inertia and shear distortion, which are ignored in the Kirchhoff plate theory. The effects of shear distortion rotatory inertia become increasingly important for propagating waves

with shorter wavelengths at high frequencies. Generally, the effect of shear distortion is more significant than that of rotatory inertia on the transverse vibration of a plate [7].

The equation of out-of-plane motion in the Mindlin plate can be obtained by using the Hamilton's variational principle. The Lagrangian is defined by subtracting the potential energy from the kinetic energy. In the Mindlin plate, the kinetic and potential energy can be represented as, respectively,

$$\mathrm{KE} = \frac{1}{2}\iint_R \left[\rho h\left(\frac{\partial w}{\partial t}\right)^2 + \rho I\left\{\left(\frac{\partial \alpha_x}{\partial t}\right)^2 + \left(\frac{\partial \alpha_y}{\partial t}\right)^2\right\}\right] \mathrm{d}A \tag{1}$$

and

$$\mathrm{PE} = \frac{1}{2}\iint_R \left\{ D\left[\left(\frac{\partial \alpha_x}{\partial x}\right)^2 + \left(\frac{\partial \alpha_y}{\partial y}\right)^2 + 2v\frac{\partial \alpha_x}{\partial x}\frac{\partial \alpha_y}{\partial y}\right] + GI\left(\frac{\partial \alpha_x}{\partial y} + \frac{\partial \alpha_y}{\partial x}\right)^2 + \kappa Gh\left(\frac{\partial w}{\partial x} - \alpha_x\right)^2 + \kappa Gh\left(\frac{\partial w}{\partial y} - \alpha_y\right)^2 \right\} \mathrm{d}A, \tag{2}$$

where w is the transverse displacement, α_x and α_y are the angles of rotation due to bending, ρ is the density, h is the thickness, $I = h^3/12$ is the moment of inertia per unit width, $D = Eh^3/[12(1-v^2)]$ is the flexural rigidity, v is Poisson's ratio, E is Young's modulus, $\kappa = 20(1+v)/(24+25v+v^2)$ is the shear correction factor and $G = E/[2(1+v)]$ is the elastic modulus of shear of the plate. Using the Hamilton's variational principle in the Lagrangian obtained by Eqs. (1) and (2), the equations of out-of-plane motion in the unloaded Mindlin plate are obtained by [34]

$$D\left[\frac{\partial^2 \alpha_x}{\partial x^2} + \frac{(1-v)}{2}\frac{\partial^2 \alpha_x}{\partial y^2} + \frac{(1+v)}{2}\frac{\partial^2 \alpha_y}{\partial x \partial y}\right] + \kappa Gh\left(\frac{\partial w}{\partial x} - \alpha_x\right) - I\rho\frac{\partial^2 \alpha_x}{\partial t^2} = 0, \tag{3}$$

$$D\left[\frac{(1-v)}{2}\frac{\partial^2 \alpha_y}{\partial x^2} + \frac{\partial^2 \alpha_y}{\partial^2 y} + \frac{(1+v)}{2}\frac{\partial^2 \alpha_x}{\partial x \partial y}\right] + \kappa Gh\left(\frac{\partial w}{\partial y} - \alpha_y\right) - I\rho\frac{\partial^2 \alpha_y}{\partial t^2} = 0, \tag{4}$$

and

$$-\kappa Gh\left(\frac{\partial^2 w}{\partial x^2} + \frac{\partial^2 w}{\partial y^2} - \frac{\partial \alpha_x}{\partial x} - \frac{\partial \alpha_y}{\partial y}\right) + \rho h\frac{\partial w^2}{\partial t^2} = 0. \tag{5}$$

3. Group velocity of out-of-plane wave in the Mindlin plate

To obtain the general solution for the homogeneous undamped problem of out-of-plane motion in the Mindlin plate [35], we can define the displacement potential functions ϕ and ψ by, respectively,

$$\alpha_x = \frac{\partial \phi}{\partial x} + \frac{\partial \psi}{\partial y}, \quad \text{and} \quad \alpha_y = \frac{\partial \phi}{\partial y} - \frac{\partial \psi}{\partial x}. \tag{6,7}$$

Using these displacement potential functions, the equations of out-of-plane motion in the Mindlin plate can be written in the form:

$$D\nabla^2\phi + \kappa Gh(w - \phi) - I\rho\frac{\partial^2 \phi}{\partial t^2} = 0, \tag{8}$$

$$D\left[\frac{(1-v)}{2}\nabla^2\psi\right] - \kappa Gh(\psi) - I\rho\frac{\partial^2 \psi}{\partial t^2} = 0, \tag{9}$$

and

$$-\kappa Gh(\nabla^2 w - \nabla^2\phi) + \rho h\frac{\partial^2 w}{\partial t^2} = 0. \tag{10}$$

From Eqs. (6) and (7), it follows that

$$\nabla^2\phi = \frac{\partial\alpha_x}{\partial x} + \frac{\partial\alpha_y}{\partial y} \quad \text{and} \quad \nabla^2\psi = \frac{\partial\gamma_{xz}}{\partial y} - \frac{\partial\gamma_{yz}}{\partial x}, \tag{11,12}$$

where $\gamma_{xz} = \partial w/\partial x - \alpha_x$ and $\gamma_{yz} = \partial w/\partial y - \alpha_y$ are shear strains.

Thus displacement potential function ϕ involves both shear distortion and rotatory inertia, whereas ψ is a function of shear alone [35]. Eq. (9) related to ψ is not coupled with the other variables and can be represented as, for time-harmonic motion,

$$\nabla^2\psi + \left(\frac{\rho I\omega^2 - \kappa Gh}{GI}\right)\psi = 0. \tag{13}$$

The general solution of Eq. (13), which is a far-field solution for $\omega > \omega_{c1}$, is

$$\psi(x,y,t) = (Ae^{-jk_{1x}x} + Be^{jk_{1x}x})(Ce^{-jk_{1y}x} + De^{jk_{1y}x})\,e^{j\omega t}, \tag{14}$$

where ω is the excitation frequency, $\omega_{c1} = \sqrt{\kappa Gh/\rho I}$ is the critical frequency of the displacement potential function wave ψ with wavenumber $k_1 = \sqrt{(\rho I\omega^2 - \kappa Gh)/GI}$, and k_{1x} and k_{1y} are x- and y-directional components of wavenumber k_1, respectively.

The wavenumber k_1 of the displacement potential function ψ above the critical frequency ($\omega > \omega_{c1}$) can be approximated as

$$k_1 = \sqrt{(\rho I\omega^2 - \kappa Gh)/GI} \approx \sqrt{\rho\omega^2/G}. \tag{15}$$

By Eqs. (12) and (15), because the displacement potential function ψ with wavenumber k_1 includes only the effect of shear distortion, this wave can be called out-of-plane shear wave (OPSW) to avoid the confusion with the shear wave of in-plane waves in a plate. From now on, the wave with wavenumber k_1 is designated as OPSW in this paper for the definite distinction among propagating waves in the Mindlin plate.

The general solution of Eqs. (8) and (10) for time-harmonic motion can be represented as

$$\begin{Bmatrix} \phi \\ w \end{Bmatrix} = C\vec{d}\,\exp(K_x x + K_y y)\,e^{j\omega t}, \tag{16}$$

where C is the constant coefficient, $\vec{d}$ is a vector of a constant number, and $K^2 = K_x{}^2 + K_y{}^2$ is a square wavenumber which is the sum of square wavenumbers of x- and y-directional wave components.

When Eq. (16) is substituted into Eqs. (8) and (10), the following matrix equation is obtained:

$$\begin{bmatrix} DK^2 - \kappa Gh + \rho I\omega^2 & \kappa Gh \\ \kappa GhK^2 & -\kappa GhK^2 - \rho h\omega^2 \end{bmatrix}\vec{d} = 0. \tag{17}$$

To have a non-trivial solution, the following characteristic equation is obtained from the upper matrix equation:

$$K^4 + \rho\omega^2\left(\frac{1}{\kappa G} + \frac{I}{D}\right)K^2 + \rho\omega^2\left(\frac{\rho I\omega^2}{\kappa GD} - \frac{h}{D}\right) = 0. \tag{18}$$

For Eq. (18), the four roots are given by

$$K = \pm\sqrt{-\frac{\rho\omega^2}{2}\left(\frac{1}{\kappa G} + \frac{I}{D}\right) \pm \sqrt{\frac{\rho^2\omega^4}{4}\left(\frac{1}{\kappa G} - \frac{I}{D}\right)^2 + \frac{\rho h\omega^2}{D}}}. \tag{19}$$

Out of the four roots, the two roots,

$$K_1 = \pm\sqrt{-\frac{\rho\omega^2}{2}\left(\frac{1}{\kappa G} + \frac{I}{D}\right) - \sqrt{\frac{\rho^2\omega^4}{4}\left(\frac{1}{\kappa G} - \frac{I}{D}\right)^2 + \frac{\rho h\omega^2}{D}}} \tag{20}$$

are always imaginary, and the other two roots,

$$K_2 = \pm\sqrt{-\frac{\rho\omega^2}{2}\left(\frac{1}{\kappa G}+\frac{I}{D}\right)+\sqrt{\frac{\rho^2\omega^4}{4}\left(\frac{1}{\kappa G}-\frac{I}{D}\right)^2+\frac{\rho h\omega^2}{D}}} \tag{21}$$

are either real or imaginary depending on the frequency ω. Therefore, the critical frequency determining whether these roots are real or imaginary exists in variables ϕ and w, and can be obtained by $\omega_{c2} = \sqrt{\kappa G h/\rho I}$. This critical frequency of the displacement potential function ϕ and transverse displacement w is identical with that of the displacement potential function ψ. Therefore, only a critical frequency for out-of-plane waves in the Mindlin plate exists and can be represented as $\omega_c = \sqrt{\kappa G h/\rho I}$. In case of a steel plate ($E = 19.8 \times 10^{10}$ Pa, $\rho = 7800$ kg, $v = 0.28$) of $h = 0.01$ m, the critical frequency of the plate is about $f_c = 156$ kHz.

In the fourth root term of Eq. (19), the term $\rho h\omega^2/D$, which is identical with the fourth power of the bending wavenumber in the Kirchhoff plate, can be regarded as that related to the effect of bending and the term of $\rho^2\omega^4(1/\kappa G - I/D)^2/4$ can be regarded as that related to the effect of shear distortion, as shown in Fig. 1. When $\omega \leqslant \omega_c$, the term related to bending effect grows dominant to that related to shear effect in Eq. (20), as frequency decreases. When $\omega > \omega_c$, the term related to shear effect grows dominant to that related to bending effect in Eqs. (20) and (21), as frequency increases.

Therefore, below the critical frequency ($\omega \leqslant \omega_c$), only the wave with wavenumber k_2 is the far-field solution and its wavenumber can be approximated as

$$k_2 = \sqrt{\frac{\rho\omega^2}{2}\left(\frac{1}{\kappa G}+\frac{I}{D}\right)+\sqrt{\frac{\rho^2\omega^4}{4}\left(\frac{1}{\kappa G}-\frac{I}{D}\right)^2+\frac{\rho h\omega^2}{D}}} \approx \sqrt[4]{\frac{\rho h\omega^2}{D}}, \tag{22}$$

where $K_1 = \pm \mathrm{j}k_2$.

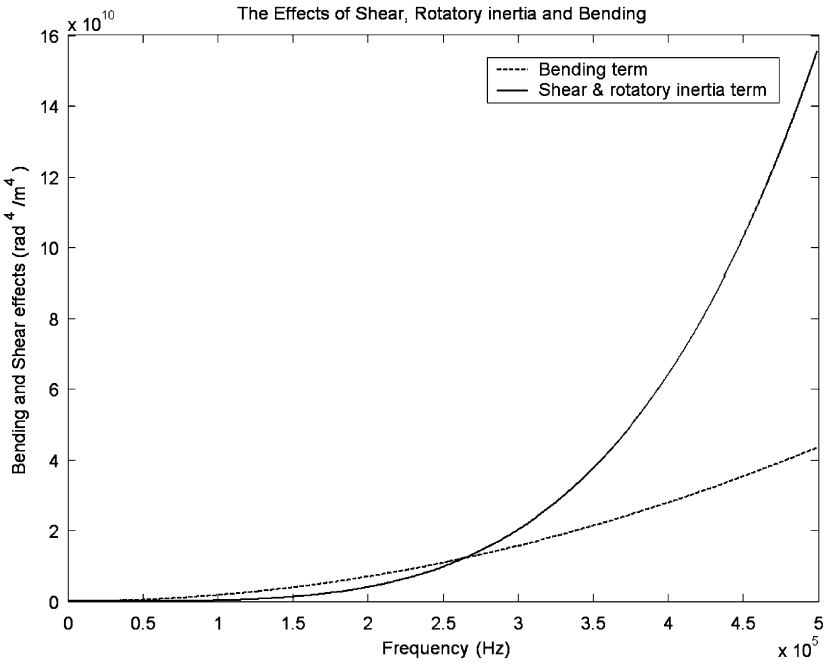

Fig. 1. The effects of shear, rotatory inertia, and bending on out-of-plane wavenumbers k_2 and k_3 of the Mindlin plate (steel, $h = 0.01$ m, $f_c = 156$ kHz); '——' is bending term and '----' is shear & rotatory inertia term.

Above the critical frequency ($\omega > \omega_c$), both kinds of waves with wavenumbers k_2 and k_3 are far-field solutions and their wavenumbers can be approximated as, respectively,

$$k_2 = \sqrt{\frac{\rho\omega^2}{2}\left(\frac{1}{\kappa G}+\frac{I}{D}\right) + \sqrt{\frac{\rho^2\omega^4}{4}\left(\frac{1}{\kappa G}-\frac{I}{D}\right)^2 + \frac{\rho h\omega^2}{D}}} \approx \sqrt{\frac{\rho\omega^2}{\kappa G}}, \tag{23}$$

and

$$k_3 = \sqrt{\frac{\rho\omega^2}{2}\left(\frac{1}{\kappa G}+\frac{I}{D}\right) - \sqrt{\frac{\rho^2\omega^4}{4}\left(\frac{1}{\kappa G}-\frac{I}{D}\right)^2 + \frac{\rho h\omega^2}{D}}} \approx \sqrt{\frac{\rho I\omega^2}{D}}, \tag{24}$$

where $K_1 = \pm \mathrm{j}k_2$ and $K_2 = \pm \mathrm{j}k_3$.

The displacement variables ϕ and w are composed of two kinds of propagating waves above the critical frequency and one kind of propagating wave below the critical frequency. Generally, the general solution of displacement variables ϕ and w can be represented as

$$\begin{Bmatrix} \phi(x,y,t) \\ w(x,y,t) \end{Bmatrix} = \left(A_1 \mathrm{e}^{-\mathrm{j}k_{2x}x} + B_1 \mathrm{e}^{\mathrm{j}k_{2x}x} + C_1 \mathrm{e}^{-\mathrm{j}k_{3x}x} + D_1 \mathrm{e}^{\mathrm{j}k_{3x}x}\right)\left(A_2 \mathrm{e}^{-\mathrm{j}k_{2y}y} + B_2 \mathrm{e}^{\mathrm{j}k_{2y}y} + C_2 \mathrm{e}^{-\mathrm{j}k_{3y}y} + D_2 \mathrm{e}^{\mathrm{j}k_{3y}y}\right)\mathrm{e}^{\mathrm{j}\omega t}, \tag{25}$$

where A_i, B_i, C_i and D_i are vectors of a constant number.

However, every combination of x- and y-components in Eq. (25) is not an appropriate solution. The other terms except the combination of x- and y-components of the same wavenumber are extraneous solutions. Therefore, using one of the eigenvectors in Eq. (17), the appropriate general solution of displacement variables ϕ and w is obtained by

$$\begin{Bmatrix} \phi \\ w \end{Bmatrix} = \left[\begin{Bmatrix} \rho h\omega^2 - \kappa G h k_2^2 \\ -\kappa G h k_2^2 \end{Bmatrix} \left(\bar{A}\mathrm{e}^{(-\mathrm{j}k_{2x}x - \mathrm{j}k_{2y}y)} + \bar{B}\mathrm{e}^{(-\mathrm{j}k_{2x}x + \mathrm{j}k_{2y}y)} + \bar{C}\mathrm{e}^{(\mathrm{j}k_{2x}x - \mathrm{j}k_{2y}y)} + \bar{D}e^{(\mathrm{j}k_{2x}x + \mathrm{j}k_{2y}y)}\right) + \begin{Bmatrix} \rho h\omega^2 - \kappa G h k_3^2 \\ -\kappa G h k_3^2 \end{Bmatrix} \left(\bar{E}\mathrm{e}^{(-\mathrm{j}k_{3x}x - \mathrm{j}k_{3y}y)} + \bar{F}\mathrm{e}^{(-\mathrm{j}k_{3x}x + \mathrm{j}k_{3y}y)} + \bar{G}\mathrm{e}^{(\mathrm{j}k_{3x}x - \mathrm{j}k_{3y}y)} + \bar{H}\mathrm{e}^{(\mathrm{j}k_{3x}x + \mathrm{j}k_{3y}y)}\right) \right] \mathrm{e}^{\mathrm{j}\omega t}. \tag{26}$$

In Eq. (26), the out-of-plane wave with wavenumber k_2 is influenced by bending below the critical frequency and by shear above the critical frequency. On the other hand, the out-of-plane wave with wavenumber k_3 propagates only above the critical frequency where the effect of shear is dominant. Based on these characteristics of out-of-plane waves except OPSW, the out-of-plane waves with wavenumbers k_2 and k_3 can be called bending dominant flexural wave (BDFW) and shear dominant flexural wave (SDFW), respectively. In this paper, the out-of-plane waves with wavenumbers k_2 and k_3 are designated as BDFW and SDFW, respectively. Additionally, though the effect of rotatory inertia is important above the critical frequency, the out-of-plane wave with wavenumber k_3 is named SDFW because the effect of shear is predominant to that of rotatory inertia.

Above the critical frequency, because three kinds of propagating waves exist, three kinds of group velocities for far-field solutions can be obtained. On the other hand, only one kind of group velocity for a far-field solution is obtained below the critical frequency.

The group velocity of OPSW with wavenumber k_1 can be represented as the derivative

$$c_{g1} = \frac{\partial\omega}{\partial k_1} = \frac{Gk_1}{\rho\omega} = \frac{G}{\rho\omega}\sqrt{\frac{\rho I\omega^2 - \kappa G h}{GI}}. \tag{27}$$

Similarly, the group velocities of BDFW and SDFW with wavenumbers k_2 and k_3 can be represented as the following derivatives, respectively,

$$c_{g2} = \frac{\partial\omega}{\partial k_2} = \frac{2k_2^3\kappa GD - k_2\rho\omega^2(D+\kappa GI)}{k_2^2\rho\omega(D+\kappa GI) - 2\rho^2\omega^3 I + \rho h\omega\kappa G} \tag{28}$$

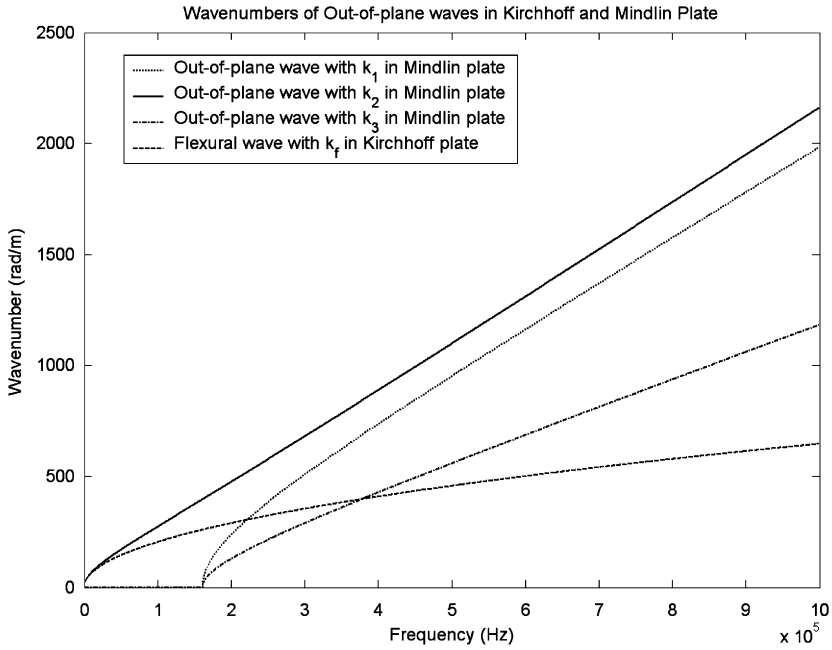

Fig. 2. The wavenumbers of propagating out-of-plane waves in steel Mindlin and Kirchhoff plates of $h = 0.01$ m: ·····, out-of-plane wave with k_1 in the Mindlin plate; ——, out-of-plane wave with k_2 in the Mindlin plate; - - - - -, out-of-plane wave with k_3 in the Mindlin plate; - - - -, flexural wave with k_f in the Kirchhoff plate.

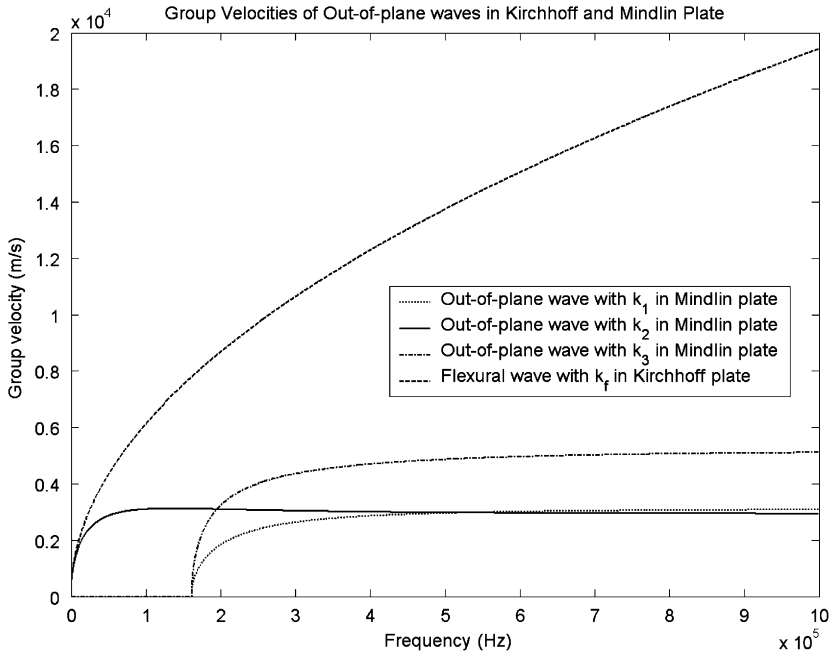

Fig. 3. The group velocities of propagating out-of-plane waves in steel Mindlin and Kirchhoff plates of $h = 0.01$ m: ·····, out-of-plane wave with k_1 in the Mindlin plate; ——, out-of-plane wave with k_2 in the Mindlin plate; - - - - -, out-of-plane wave with k_3 in the Mindlin plate; - - - -, flexural wave with k_f in the Kirchhoff plate.

and

$$c_{g3} = \frac{\partial \omega}{\partial k_3} = \frac{2k_3^3 \kappa GD - k_3 \rho \omega^2 (D + \kappa GI)}{k_3^2 \rho \omega (D + \kappa GI) - 2\rho^2 \omega^3 I + \rho h \omega \kappa G}. \tag{29}$$

In case of the Kirchhoff plate, the group velocity of a flexural wave is given by

$$c_{gK} = \frac{\partial \omega}{\partial k_f} = 2\left(\frac{D\omega^2}{\rho h}\right)^{1/4}, \tag{30}$$

where $k_f = (\rho h \omega^2 / D)^{1/4}$ is the flexural wavenumber in the Kirchhoff plate.

Figs. 2 and 3 show the values of wavenumbers and group velocities of propagating out-of-plane waves in steel Kirchhoff and Mindlin plates of $h = 0.01$ m, respectively, at various frequencies.

4. Derivation of time- and locally space-averaged far-field smooth energy density and intensity

4.1. Above the critical frequency

The general solution in Eqs. (14) and (26) is composed of far-field and near-field solutions. The near-field solution is important in the low-frequency range where the wavelength is short, but the solution is negligible in the high-frequency range. Noiseux showed that the far-field solution is useful for the power flow analysis of vibrating plate in the high-frequency ranges [36].

Above the critical frequency, three kinds of propagating out-of-plane waves, that is to say, OPSW, BDFW and SDFW, exist but the exponentially decaying evanescent wave, otherwise referred to as the near-field solution, does not exist. Using Eqs. (14) and (26), the far-field solutions for the out-of-plane motion in the damped Mindlin plate are represented as

$$\psi = \left\{ \bar{A}_1 e^{(-jk_{1cx}x - jk_{1cy}x)} + \bar{A}_2 e^{(-jk_{1cx}x + jk_{1cy}x)} + \bar{A}_3 e^{(jk_{1cx}x - jk_{1cy}x)} + \bar{A}_4 e^{(jk_{1cx}x + jk_{1cy}x)} \right\} e^{j\omega t} \tag{31}$$

and

$$\begin{Bmatrix} \phi \\ w \end{Bmatrix} = \left[\begin{Bmatrix} \rho h\omega^2 - \kappa G_c h k_{2c}^2 \\ -\kappa G_c h k_{2c}^2 \end{Bmatrix} \left(\bar{B}_1 e^{(-jk_{2cx}x - jk_{2cy}y)} + \bar{B}_2 e^{(-jk_{2cx}x + jk_{2cy}y)} + \bar{B}_3 e^{(jk_{2cx}x - jk_{2cy}y)} + \bar{B}_4 e^{(jk_{2cx}x + jk_{2cy}y)} \right) \right.$$
$$\left. + \begin{Bmatrix} \rho h\omega^2 - \kappa G_c h k_{3c}^2 \\ -\kappa G_c h k_{3c}^2 \end{Bmatrix} \left(\bar{C}_1 e^{(-jk_{3cx}x - jk_{3cy}y)} + \bar{C}_2 e^{(-jk_{3cx}x + jk_{3cy}y)} + \bar{C}_3 e^{(jk_{3cx}x - jk_{3cy}y)} + \bar{C}_4 e^{(jk_{3cx}x + jk_{3cy}y)} \right) \right] e^{j\omega t}, \tag{32}$$

where $\bar{A}_i$, $\bar{B}_i$ and $\bar{C}_i$ are complex coefficients, the subscripts x and y in complex wavenumbers denote x- and y-component of the wavenumber, respectively, $G_c = G(1 + j\eta)$ is the complex elastic modulus of shear, which is represented as hysteretic damping factor η, complex wavenumbers are

$$k_{1c} = \sqrt{(\rho I \omega^2 - \kappa G_c h)/G_c I}, \tag{33}$$

$$k_{2c,3c} = \sqrt{\frac{\rho\omega^2}{2}\left(\frac{1}{\kappa G_c} + \frac{I}{D_c}\right) \pm \sqrt{\frac{\rho^2\omega^4}{4}\left(\frac{1}{\kappa G_c} - \frac{I}{D_c}\right)^2 + \frac{\rho h \omega^2}{D_c}}}. \tag{34,35}$$

The total energy density is the sum of the potential and kinetic energy densities in Eqs. (1) and (2). Since the average values of energy density and intensity are more interesting than instantaneous values, the energy density and intensity are time-averaged by averaging over a period [37]. The time-averaged total energy

density for out-of-plane motion in the Mindlin plate can be represented as

$$\begin{aligned}\langle e\rangle = \mathrm{Re}\Bigg[&\frac{\rho h}{4}\left(\frac{\partial w}{\partial t}\right)\left(\frac{\partial w}{\partial t}\right)^{*}+\frac{\rho I}{4}\left\{\left(\frac{\partial \alpha_x}{\partial t}\right)\left(\frac{\partial \alpha_x}{\partial t}\right)^{*}+\left(\frac{\partial \alpha_y}{\partial t}\right)\left(\frac{\partial \alpha_y}{\partial t}\right)^{*}\right\}\\&+\frac{D}{4}\left\{\left(\frac{\partial \alpha_x}{\partial x}\right)\left(\frac{\partial \alpha_x}{\partial x}\right)^{*}+\left(\frac{\partial \alpha_y}{\partial y}\right)\left(\frac{\partial \alpha_y}{\partial y}\right)^{*}+2\nu\left(\frac{\partial \alpha_x}{\partial x}\right)\left(\frac{\partial \alpha_y}{\partial y}\right)^{*}\right\}\\&+\frac{GI}{4}\left\{\left(\frac{\partial \alpha_x}{\partial y}+\frac{\partial \alpha_y}{\partial x}\right)\left(\frac{\partial \alpha_x}{\partial y}+\frac{\partial \alpha_y}{\partial x}\right)^{*}\right\}+\frac{\kappa G h}{4}\\&\times\left\{\left(\frac{\partial w}{\partial x}-\alpha_x\right)\left(\frac{\partial w}{\partial x}-\alpha_x\right)^{*}+\left(\frac{\partial w}{\partial y}-\alpha_y\right)\left(\frac{\partial w}{\partial y}-\alpha_y\right)^{*}\right\}\Bigg],\end{aligned} \tag{36}$$

where $\langle\ \rangle$ operator indicates a time-averaged quality and the asterisk notation denotes a complex conjugate. The time-averaged total intensity for out-of-plane motion in the Mindlin plate is transmitted by the shear force and the moment, and can be represented as $\langle \mathbf{I}\rangle = \langle I_x\rangle\vec{i}+\langle I_y\rangle\vec{j}$, where

$$\begin{aligned}\langle I_x\rangle = \frac{1}{2}\mathrm{Re}\Bigg[&-D\left(\frac{\partial \alpha_x}{\partial x}+\nu\frac{\partial \alpha_y}{\partial y}\right)\left(\frac{\partial \alpha_x}{\partial t}\right)^{*}-(1-\nu)\frac{D}{2}\left(\frac{\partial \alpha_x}{\partial y}+\frac{\partial \alpha_y}{\partial x}\right)\left(\frac{\partial \alpha_y}{\partial t}\right)^{*}\\&-\kappa G h\left(\frac{\partial w}{\partial x}-\alpha_x\right)\left(\frac{\partial w}{\partial t}\right)^{*}\Bigg]\end{aligned}$$

and

$$\begin{aligned}\langle I_y\rangle = \frac{1}{2}\mathrm{Re}\Bigg[&-D\left(\frac{\partial \alpha_y}{\partial y}+\nu\frac{\partial \alpha_x}{\partial x}\right)\left(\frac{\partial \alpha_y}{\partial t}\right)^{*}-(1-\nu)\frac{D}{2}\left(\frac{\partial \alpha_x}{\partial y}+\frac{\partial \alpha_y}{\partial x}\right)\left(\frac{\partial \alpha_x}{\partial t}\right)^{*}\\&-\kappa G h\left(\frac{\partial w}{\partial y}-\alpha_y\right)\left(\frac{\partial w}{\partial t}\right)^{*}\Bigg].\end{aligned} \tag{37,38}$$

In lightly damped plates, i.e., $\eta \ll 1$, using Eqs. (33)–(35), the real and imaginary components of the complex wavenumbers $k_{1c} = k_{11}+\mathrm{j}k_{12}$, $k_{2c} = k_{21}+\mathrm{j}k_{22}$ and $k_{3c} = k_{31}+\mathrm{j}k_{32}$, respectively, are well approximated as

$$k_{11} = \sqrt{\frac{\rho I\omega^2-\kappa G h}{GI}},\quad k_{12} = -\left(\frac{\eta}{2}\right)k_{11},$$

$$k_{21,31} = \sqrt{\frac{\rho\omega^2}{2}\left(\frac{1}{\kappa G}+\frac{I}{D}\right)\pm\sqrt{\frac{\rho^2\omega^4}{4}\left(\frac{1}{\kappa G}-\frac{I}{D}\right)^2+\frac{\rho h\omega^2}{D}}}$$

and

$$k_{22,32} = -\left(\frac{\eta}{2}\right)k_{21,31} \tag{39 - 44}$$

Substituting Eqs. (6), (7), (31) and (32) into Eqs. (36)–(38), the time-averaged far-field energy density and intensity, whose primary variables are w, ϕ and ψ, are obtained (Appendix A).

Assuming that hysteretic damping for the Mindlin plate is sufficiently small, the terms on the order of square or more of η can be neglected. Additionally, the local space-average is used to eliminate the terms which are spatially harmonic in the time-averaged far-field energy density and intensity. By these procedures, the time- and locally space-averaged far-field smooth energy density and the components of the time- and locally space-averaged far-field smooth intensity of out-of-plane waves in the Mindlin plate can be

approximated as (Appendix A)

$$\begin{aligned}\langle \bar{e} \rangle = {} & \tfrac{1}{4}[(\rho I\omega^2 + \kappa Gh)k_{11}^2 + GIk_{11}^4] \\ & \times (|\bar{A}_1|^2 e^{\eta(-k_{11x}x - k_{11y}y)} + |\bar{A}_2|^2 e^{\eta(-k_{11x}x + k_{11y}y)} + |\bar{A}_3|^2 e^{\eta(k_{11x}x - k_{11y}y)} + |\bar{A}_4|^2 e^{\eta(k_{11x}x + k_{11y}y)}) \\ & + \tfrac{1}{4}[(\rho h\omega^2 - \kappa Ghk_{21}^2)^2 (Dk_{21}^4 + \rho I\omega^2 k_{21}^2) + k_{21}^2(\rho h\omega^2)(\kappa Gh)(\kappa Ghk_{21}^2 + \rho h\omega^2)] \\ & \times (|\bar{B}_1|^2 e^{\eta(-k_{21x}x - k_{21y}y)} + |\bar{B}_2|^2 e^{\eta(-k_{21x}x + k_{21y}y)} + |\bar{B}_3|^2 e^{\eta(k_{21x}x - k_{21y}y)} + |\bar{B}_4|^2 e^{\eta(k_{21x}x + k_{21y}y)}) \\ & + \tfrac{1}{4}[(\rho h\omega^2 - \kappa Ghk_{31}^2)^2 (Dk_{31}^4 + \rho I\omega^2 k_{31}^2) + k_{31}^2(\rho h\omega^2)(\kappa Gh)(\kappa Ghk_{31}^2 + \rho h\omega^2)] \\ & \times (|\bar{C}_1|^2 e^{\eta(-k_{31x}x - k_{31y}y)} + |\bar{C}_2|^2 e^{\eta(-k_{31x}x + k_{31y}y)} + |\bar{C}_3|^2 e^{\eta(k_{31x}x - k_{31y}y)} + |\bar{C}_4|^2 e^{\eta(k_{31x}x + k_{31y}y)}), \end{aligned} \tag{45}$$

$$\begin{aligned}\langle \bar{I}_x \rangle = {} & \frac{1}{2}\left[\frac{D}{2}(1-\nu)\omega k_{11x}k_{11}^2\right] \\ & \times (|\bar{A}_1|^2 e^{\eta(-k_{11x}x - k_{11y}y)} + |\bar{A}_2|^2 e^{\eta(-k_{11x}x + k_{11y}y)} - |\bar{A}_3|^2 e^{\eta(k_{11x}x - k_{11y}y)} - |\bar{A}_4|^2 e^{\eta(k_{11x}x + k_{11y}y)}) \\ & + \frac{1}{2}[D(\rho h\omega^2 - \kappa Ghk_{21}^2)^2 \omega k_{21x}k_{21}^2 + (\rho h\omega^2)(\omega k_{21x})(\kappa Ghk_{21})^2] \\ & \times (|\bar{B}_1|^2 e^{\eta(-k_{21x}x - k_{21y}y)} + |\bar{B}_2|^2 e^{\eta(-k_{21x}x + k_{21y}y)} - |\bar{B}_3|^2 e^{\eta(k_{21x}x - k_{21y}y)} - |\bar{B}_4|^2 e^{\eta(k_{21x}x + k_{21y}y)}) \\ & + \frac{1}{2}[D(\rho h\omega^2 - \kappa Ghk_{31}^2)^2 \omega k_{31x}k_{31}^2 + (\rho h\omega^2)(\omega k_{31x})(\kappa Ghk_{31})^2] \\ & \times (|\bar{C}_1|^2 e^{\eta(-k_{31x}x - k_{31y}y)} + |\bar{C}_2|^2 e^{\eta(-k_{31x}x + k_{31y}y)} - |\bar{C}_3|^2 e^{\eta(k_{31x}x - k_{31y}y)} - |\bar{C}_4|^2 e^{\eta(k_{31x}x + k_{31y}y)}) \end{aligned} \tag{46}$$

and

$$\begin{aligned}\langle \bar{I}_y \rangle = {} & \frac{1}{2}\left[\frac{D}{2}(1-\nu)\omega k_{11y}k_{11}^2\right] \\ & \times (|\bar{A}_1|^2 e^{\eta(-k_{11x}x - k_{11y}y)} - |\bar{A}_2|^2 e^{\eta(-k_{11x}x + k_{11y}y)} + |\bar{A}_3|^2 e^{\eta(k_{11x}x - k_{11y}y)} - |\bar{A}_4|^2 e^{\eta(k_{11x}x + k_{11y}y)}) \\ & + \frac{1}{2}[D(\rho h\omega^2 - \kappa Ghk_{21}^2)^2 \omega k_{21y}k_{21}^2 + (\rho h\omega^2)(\omega k_{21y})(\kappa Ghk_{21})^2] \\ & \times (|\bar{B}_1|^2 e^{\eta(-k_{21x}x - k_{21y}y)} - |\bar{B}_2|^2 e^{\eta(-k_{21x}x + k_{21y}y)} + |\bar{B}_3|^2 e^{\eta(k_{21x}x - k_{21y}y)} - |\bar{B}_4|^2 e^{\eta(k_{21x}x + k_{21y}y)}) \\ & + \frac{1}{2}[D(\rho h\omega^2 - \kappa Ghk_{31}^2)^2 \omega k_{31y}k_{31}^2 + (\rho h\omega^2)(\omega k_{31y})(\kappa Ghk_{31})^2] \\ & \times (|\bar{C}_1|^2 e^{\eta(-k_{31x}x - k_{31y}y)} - |\bar{C}_2|^2 e^{\eta(-k_{31x}x + k_{31y}y)} + |\bar{C}_3|^2 e^{\eta(k_{31x}x - k_{31y}y)} - |\bar{C}_4|^2 e^{\eta(k_{31x}x + k_{31y}y)}), \end{aligned} \tag{47}$$

where $\langle \cdot \rangle$ means the time- and locally space-averaged quantity.

As shown in Eqs. (45)–(47), above the critical frequency, the time- and locally space-averaged far-field smooth energy density and intensity of out-of-plane waves can be separated into the terms of each kind of propagating wave, which is OPSW, BDFW or SDFW.

4.2. Below the critical frequency

When $\omega \leqslant \omega_c$, only one kind of out-of-plane wave, BDFW, is the far-field solution and the other kinds of waves are near-field solutions. Therefore, below the critical frequency, the far-field solution neglecting near-field solutions is given by

$$\begin{Bmatrix} \phi \\ w \end{Bmatrix} = \begin{Bmatrix} \rho h\omega^2 - \kappa G_c h k_{2c}^2 \\ -\kappa G_c h k_{2c}^2 \end{Bmatrix} (\bar{B}_1 e^{(-jk_{2cx}x - jk_{2cy}y)} + \bar{B}_2 e^{(-jk_{2cx}x + jk_{2cy}y)} + \bar{B}_3 e^{(jk_{2cx}x - jk_{2cy}y)} + \bar{B}_4 e^{(jk_{2cx}x + jk_{2cy}y)})\, e^{j\omega t}. \tag{48}$$

The displacement potential function ψ, OPSW, is a near-field solution and is neglected in the far-field energetics.

In lightly damped plates, using Eq. (34), because the effect of bending is dominant in these frequency ranges, the real and imaginary components of the complex wavenumber $k_{2c} = k_{21} + jk_{22}$, respectively, are well

approximated as

$$k_{21} = \sqrt{\frac{\rho\omega^2}{2}\left(\frac{1}{\kappa G}+\frac{I}{D}\right) + \sqrt{\frac{\rho^2\omega^4}{4}\left(\frac{1}{\kappa G}-\frac{I}{D}\right)^2 + \frac{\rho h\omega^2}{D}}},$$

and

$$k_{22} = -\left(\frac{\eta}{4}\right)k_{21}. \tag{49,50}$$

Like the former case above the critical frequency, substituting Eqs. (6), (7) and (48) into Eqs. (36)–(38), the time-averaged far-field energy density and the components of the time-averaged far-field intensity for BDFW are obtained. Assuming that hysteretic damping is sufficiently small ($\eta \ll 1$), the terms on the order of square or more of η are neglected. The local space-average is also used to eliminate the terms which are spatially harmonic in the time-averaged energy density and intensity. Below the critical frequency, the time- and locally space-averaged far-field smooth energy density and the components of the time- and locally space-averaged far-field smooth intensity for out-of-plane waves in the Mindlin plate can be approximated as (Appendix A)

$$\begin{aligned}\langle \bar{e} \rangle = {} & \tfrac{1}{4}[(\rho h\omega^2 - \kappa G h k_{21}^2)^2 (D k_{21}^4 + \rho I \omega^2 k_{21}^2) + k_{21}^2 (\rho h\omega^2)(\kappa G h)(\kappa G h k_{21}^2 + \rho h\omega^2)] \\ & \times (|[\bar{B}_1]^{++}|^2 + |[\bar{B}_2]^{+-}|^2 + |[\bar{B}_3]^{-+}|^2 + |[\bar{B}_4]^{--}|^2),\end{aligned} \tag{51}$$

$$\begin{aligned}\langle \bar{I}_x \rangle = {} & \tfrac{1}{2}[D(\rho h\omega^2 - \kappa G h k_{21}^2)^2 \omega k_{21x} k_{21}^2 + (\rho h\omega^2)(\omega k_{21x})(\kappa G h k_{21})^2] \\ & \times (|[\bar{B}_1]^{++}|^2 + |[\bar{B}_2]^{+-}|^2 - |[\bar{B}_3]^{-+}|^2 - |[\bar{B}_4]^{--}|^2)\end{aligned} \tag{52}$$

and

$$\begin{aligned}\langle \bar{I}_y \rangle = {} & \tfrac{1}{2}[D(\rho h\omega^2 - \kappa G h k_{21}^2)^2 \omega k_{21y} k_{21}^2 + (\rho h\omega^2)(\omega k_{21y})(\kappa G h k_{21})^2] \\ & \times (|[\bar{B}_1]^{++}|^2 - |[\bar{B}_2]^{+-}|^2 + |[\bar{B}_3]^{-+}|^2 - |[\bar{B}_4]^{--}|^2),\end{aligned} \tag{53}$$

where $|[\,]^{\pm\pm}|^2 = [\,]^2 \times \exp\{2(\pm k_{22x}x \pm k_{22y}y)\}$.

As shown in Eqs. (51)–(53), below the critical frequency, the time- and locally space-averaged far-field smooth energy density and the components of the time- and locally space-averaged far-field smooth intensity are expressed in only terms related to BDFW with wavenumber k_2, which is similar to the energetics of the flexural wave in the Kirchhoff plate model.

5. Derivation of energy governing equations for out-of-plane waves in the Mindlin plate

5.1. Above the critical frequency

Above the critical frequency, the time- and locally space-averaged far-field smooth energy density and intensity, which are expressed by Eqs. (45), and (46)–(47), respectively, are composed of three kinds of out-of-plane waves, OPSW, BDFW and SDFW. Both far-field smooth energy density and intensity can be separated into the terms of each out-of-plane wave. Therefore, the time- and locally space-averaged total far-field smooth energy density and intensity are expressed as, respectively,

$$\langle \bar{e} \rangle = \langle \bar{e}_1 \rangle + \langle \bar{e}_2 \rangle + \langle \bar{e}_3 \rangle \tag{54}$$

and

$$\langle \bar{\mathbf{I}} \rangle = \langle \bar{\mathbf{I}}_1 \rangle + \langle \bar{\mathbf{I}}_2 \rangle + \langle \bar{\mathbf{I}}_3 \rangle. \tag{55}$$

In Eqs. (54) and (55), "1", "2" and "3" in the subscripts denote OPSW, BDFW and SDFW, respectively.

The time- and locally space-averaged far-field smooth energy density and intensity of OPSW with wavenumber k_{1c} are given by, respectively,

$$\langle \bar{e}_1 \rangle = \frac{1}{4}[(\rho I\omega^2 + \kappa G h)k_{11}^2 + G I k_{11}^4] \times (|[\bar{A}_1]^{++}|^2 + |[\bar{A}_2]^{+-}|^2 + |[\bar{A}_3]^{-+}|^2 + |[\bar{A}_4]^{--}|^2), \tag{56}$$

$$\langle \bar{I}_{1x} \rangle = \frac{1}{2}\left[\frac{D}{2}(1-\nu)\omega k_{11x} k_{11}^2\right] \times (|[\bar{A}_1]^{++}|^2 + |[\bar{A}_2]^{+-}|^2 - |[\bar{A}_3]^{-+}|^2 - |[\bar{A}_4]^{--}|^2), \tag{57}$$

and

$$\langle \bar{I}_{1y} \rangle = \frac{1}{2}\left[\frac{D}{2}(1-\nu)\omega k_{11y} k_{11}^2\right] \times (|[\bar{A}_1]^{++}|^2 - |[\bar{A}_2]^{+-}|^2 + |[\bar{A}_3]^{-+}|^2 - |[\bar{A}_4]^{--}|^2), \tag{58}$$

where $|[\,]^{\pm\pm}|^2 = [\,]^2 \times \exp\{2(\pm k_{12x}x \pm k_{12y}y)\}$.

The time- and locally space-averaged far-field smooth energy density and intensity of BDFW with wavenumber k_{2c} are given by, respectively,

$$\langle \bar{e}_2 \rangle = \frac{1}{4}[(\rho h\omega^2 - \kappa G h k_{21}^2)^2 (D k_{21}^4 + \rho I \omega^2 k_{21}^2) + k_{21}^2 (\rho h\omega^2)(\kappa G h)(\kappa G h k_{21}^2 + \rho h\omega^2)] \times (|[\bar{B}_1]^{++}|^2 + |[\bar{B}_2]^{+-}|^2 + |[\bar{B}_3]^{-+}|^2 + |[\bar{B}_4]^{--}|^2), \tag{59}$$

$$\langle \bar{I}_{2x} \rangle = \frac{1}{2}[D(\rho h\omega^2 - \kappa G h k_{21}^2)^2 \omega k_{21x} k_{21}^2 + (\rho h\omega^2)(\omega k_{21x})(\kappa G h k_{21})^2] \times (|[\bar{B}_1]^{++}|^2 + |[\bar{B}_2]^{+-}|^2 - |[\bar{B}_3]^{-+}|^2 - |[\bar{B}_4]^{--}|^2) \tag{60}$$

and

$$\langle \bar{I}_{2y} \rangle = \frac{1}{2}[D(\rho h\omega^2 - \kappa G h k_{21}^2)^2 \omega k_{21y} k_{21}^2 + (\rho h\omega^2)(\omega k_{21y})(\kappa G h k_{21})^2] \times (|[\bar{B}_1]^{++}|^2 - |[\bar{B}_2]^{+-}|^2 + |[\bar{B}_3]^{-+}|^2 - |[\bar{B}_4]^{--}|^2), \tag{61}$$

where $|[\,]^{\pm\pm}|^2 = [\,]^2 \times \exp\{2(\pm k_{22x}x \pm k_{22y}y)\}$.

The time- and locally space-averaged far-field smooth energy density and intensity of SDFW with wavenumber k_{3c} are given by, respectively,

$$\langle \bar{e}_3 \rangle = \frac{1}{4}[(\rho h\omega^2 - \kappa G h k_{31}^2)^2 (D k_{31}^4 + \rho I \omega^2 k_{31}^2) + k_{31}^2 (\rho h\omega^2)(\kappa G h)(\kappa G h k_{31}^2 + \rho h\omega^2)] \times (|[\bar{C}_1]^{++}|^2 + |[\bar{C}_2]^{+-}|^2 + |[\bar{C}_3]^{-+}|^2 + |[\bar{C}_4]^{--}|^2), \tag{62}$$

$$\langle \bar{I}_{3x} \rangle = \frac{1}{2}[D(\rho h\omega^2 - \kappa G h k_{31}^2)^2 \omega k_{31x} k_{31}^2 + (\rho h\omega^2)(\omega k_{31x})(\kappa G h k_{31})^2] \times (|[\bar{C}_1]^{++}|^2 + |[\bar{C}_2]^{+-}|^2 - |[\bar{C}_3]^{-+}|^2 - |[\bar{C}_4]^{--}|^2) \tag{63}$$

and

$$\langle \bar{I}_{3y} \rangle = \frac{1}{2}[D(\rho h\omega^2 - \kappa G h k_{31}^2)^2 \omega k_{31y} k_{31}^2 + (\rho h\omega^2)(\omega k_{31y})(\kappa G h k_{31})^2] \times (|[\bar{C}_1]^{++}|^2 - |[\bar{C}_2]^{+-}|^2 + |[\bar{C}_3]^{-+}|^2 - |[\bar{C}_4]^{--}|^2), \tag{64}$$

where $|[]^{\pm\pm}|^2 = []^2 \times \exp\{2(\pm k_{32x}x \pm k_{32y}y)\}$.

Above the critical frequency, because the effect of shear is dominant to that of bending, the squares of k_{11}, k_{21} and k_{31}, which are the real parts of the wavenumbers, can be approximated as, respectively,

$$k_{11}^2 \approx \frac{\rho\omega^2}{G}, \quad k_{21}^2 \approx \frac{\rho\omega^2}{\kappa G}, \quad \text{and} \quad k_{31}^2 \approx \frac{\rho I \omega^2}{D}. \tag{65–67}$$

Using Eqs. (65)–(67), the group velocities of OPSW, BDFW and SDFW can be approximated by, respectively,

$$c_{g1} = \frac{\partial\omega}{\partial k_{11}} \approx \frac{G}{\rho\omega k_{11}} = \sqrt{\frac{G}{\rho}}, \tag{68}$$

$$c_{g2} = \frac{\partial\omega}{\partial k_{21}} \approx \frac{\kappa G k_{21}}{\rho\omega} = \frac{\kappa G}{\rho\omega}\sqrt{\frac{\rho\omega^2}{2}\left(\frac{1}{\kappa G}+\frac{I}{D}\right)+\sqrt{\frac{\rho^2\omega^4}{4}\left(\frac{1}{\kappa G}-\frac{I}{D}\right)^2+\frac{\rho h\omega^2}{D}}}, \tag{69}$$

and

$$c_{g3} = \frac{\partial\omega}{\partial k_{31}} \approx \frac{D k_{31}}{\rho I\omega} = \frac{D}{\rho I\omega}\sqrt{\frac{\rho\omega^2}{2}\left(\frac{1}{\kappa G}+\frac{I}{D}\right)-\sqrt{\frac{\rho^2\omega^4}{4}\left(\frac{1}{\kappa G}-\frac{I}{D}\right)^2+\frac{\rho h\omega^2}{D}}}. \tag{70}$$

Substituting Eqs. (65)–(67) into Eqs. (56)–(64), the relationships between the time- and locally space-averaged far-field smooth energy density and intensity of each propagating out-of-plane waves are derived by, respectively,

$$\langle \bar{\mathrm{I}}_1\rangle = -\frac{c_{g1}^2}{\eta\omega}\left(\frac{\partial}{\partial x}\vec{i}+\frac{\partial}{\partial y}\vec{j}\right)\langle \bar{e}_1\rangle, \tag{71}$$

$$\langle \bar{\mathrm{I}}_2\rangle = -\frac{c_{g2}^2}{\eta\omega}\left(\frac{\partial}{\partial x}\vec{i}+\frac{\partial}{\partial y}\vec{j}\right)\langle \bar{e}_2\rangle \tag{72}$$

and

$$\langle \bar{\mathrm{I}}_3\rangle = -\frac{c_{g3}^2}{\eta\omega}\left(\frac{\partial}{\partial x}\vec{i}+\frac{\partial}{\partial y}\vec{j}\right)\langle \bar{e}_3\rangle. \tag{73}$$

For a steady state elastic system, the power balance equation can be written as

$$\nabla\cdot \mathrm{I} + \pi_{\mathrm{diss}} = \pi_{\mathrm{in}}, \tag{74}$$

where π_{diss} and π_{in} are the dissipated power due to the damping of the system and the input power, respectively. From the works of Cremer and Heckl [7], the time-averaged dissipated power in an elastic medium with small structural hysteretic damping is proportional to the time-averaged total energy density in the form of

$$\pi_{\mathrm{diss}} = \eta\omega\langle e\rangle. \tag{75}$$

Substituting Eq. (75) into Eq. (74), the second-order partial differential equations, which set the far-field smooth energy density related to each kind of propagating wave as a primary variable, can be derived by,

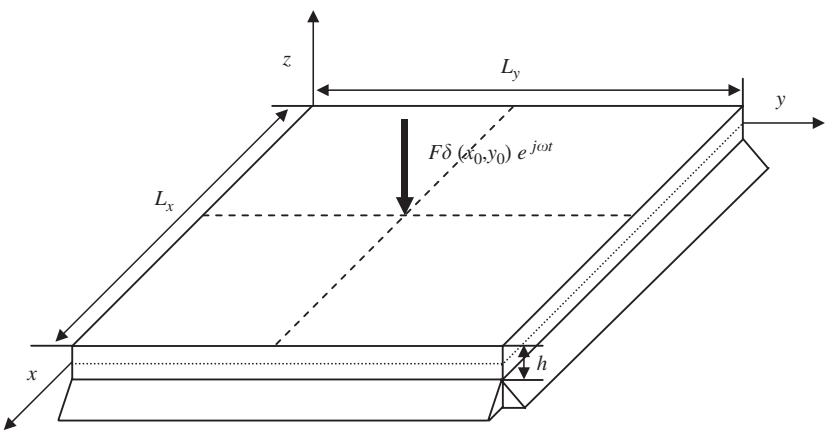

Fig. 4. Simply supported, transversely vibrating rectangular Mindlin plate excited by a harmonic point force.

respectively, using Eqs. (71)–(73),

$$-\frac{c_{g1}^2}{\eta\omega}\left(\frac{\partial^2}{\partial x^2}+\frac{\partial^2}{\partial y^2}\right)\langle\bar{e}_1\rangle+\eta\omega\langle\bar{e}_1\rangle=\pi_{1,\mathrm{in}}, \tag{76}$$

$$-\frac{c_{g2}^2}{\eta\omega}\left(\frac{\partial^2}{\partial x^2}+\frac{\partial^2}{\partial y^2}\right)\langle\bar{e}_2\rangle+\eta\omega\langle\bar{e}_2\rangle=\pi_{2,\mathrm{in}} \tag{77}$$

and

$$-\frac{c_{g3}^2}{\eta\omega}\left(\frac{\partial^2}{\partial x^2}+\frac{\partial^2}{\partial y^2}\right)\langle\bar{e}_3\rangle+\eta\omega\langle\bar{e}_3\rangle=\pi_{3,\mathrm{in}}. \tag{78}$$

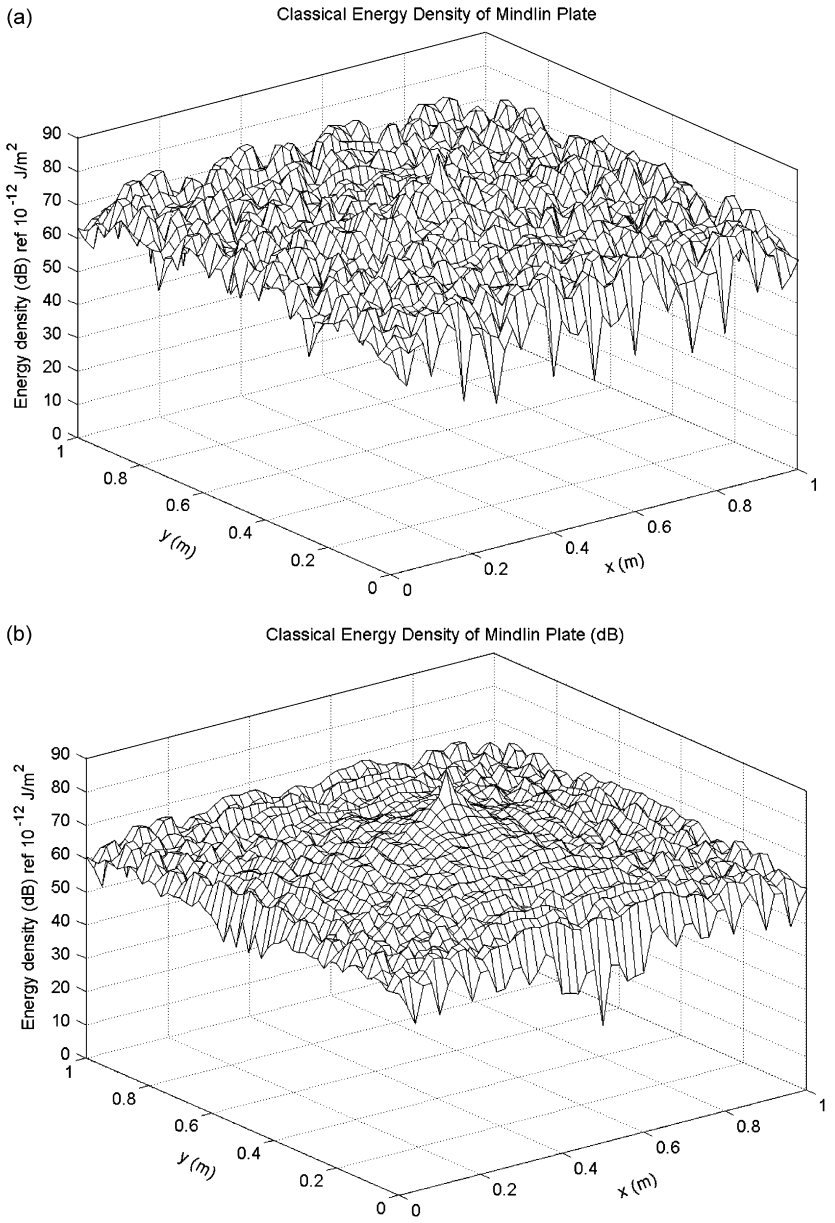

Fig. 5. The energy density level distributions of classical solutions of the Mindlin plate ($h=0.001$ m, $f_c=1.56$ MHz) when $f=1$ kHz. The reference energy density is $10^{-12}\,\mathrm{J/m^2}$: (a) $\eta=0.01$, (b) $\eta=0.1$.

5.2. Below the critical frequency

Below the critical frequency, the time- and locally space-averaged far-field smooth energy density and intensity, which are expressed by Eqs. (51), and (52) and (53), respectively, are composed of only one kind of out-of-plane wave, BDFW. In these frequency ranges, because the bending effect is dominant over the shear and rotatory effects, the wavenumber k_{21}, which is the real part of k_{2c}, can be approximated differently from k_{21} above the critical frequency by

$$k_{21} = \sqrt{\frac{\rho\omega^2}{2}\left(\frac{1}{\kappa G}+\frac{I}{D}\right) + \sqrt{\frac{\rho^2\omega^4}{4}\left(\frac{1}{\kappa G}-\frac{I}{D}\right)^2 + \frac{\rho h\omega^2}{D}}} \approx \left(\frac{\rho h\omega^2}{D}\right)^{1/4}. \tag{79}$$

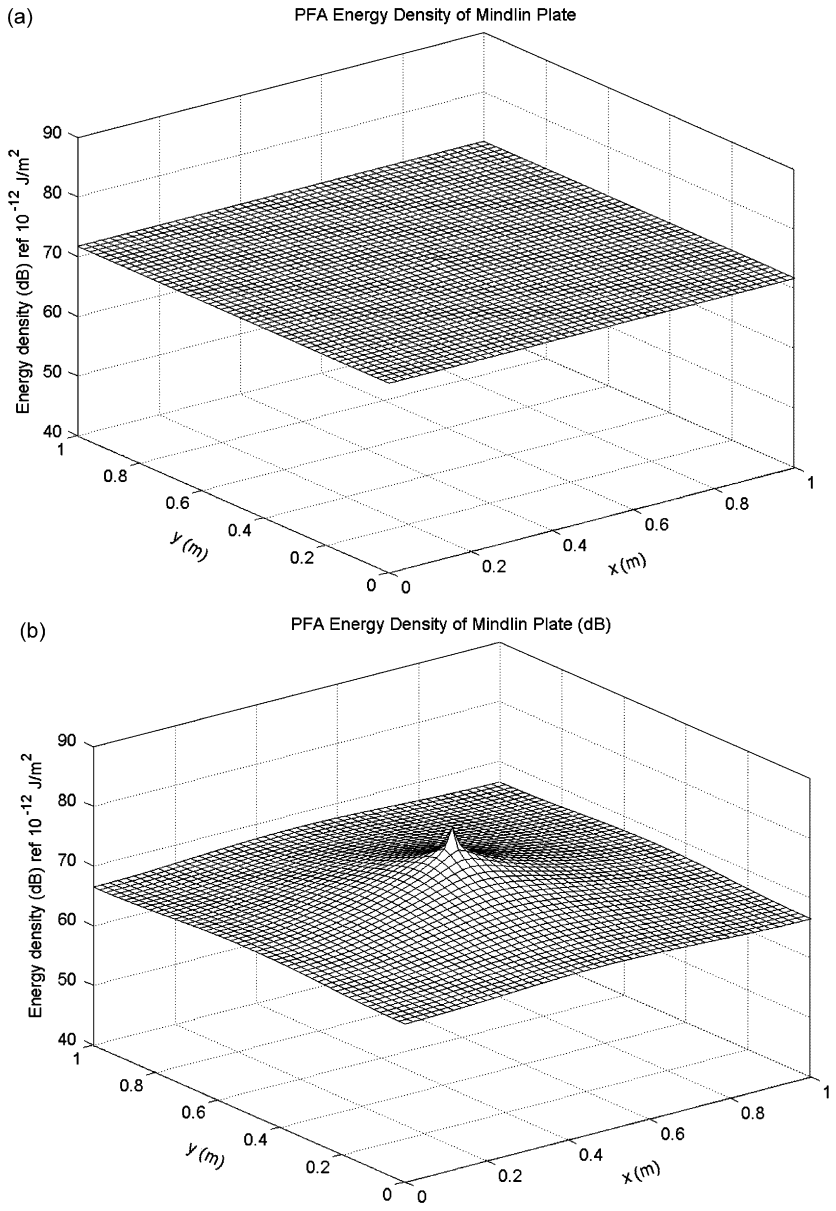

Fig. 6. The energy density level distributions of power flow solutions of the Mindlin plate ($h = 0.001$ m, $f_c = 1.56$ MHz) when $f = 1$ kHz. The reference energy density is 10^{-12} J/m^2: (a) $\eta = 0.01$, (b) $\eta = 0.1$.

Using Eq. (79), the group velocity of BDFW with wavenumber k_{2c} can be expressed by

$$c_{g2} = \frac{\partial\omega}{\partial k_{21}} \approx 2k_{21}\sqrt{\frac{D}{\rho h}} = 2\left(\frac{\rho h\omega^2}{D}\right)^{1/4}\sqrt{\frac{D}{\rho h}} = 2\left(\frac{\omega^2 D}{\rho h}\right)^{1/4}. \tag{80}$$

These approximated wavenumber and group velocity are identical to those of the flexural wave in the Kirchhoff plate. Substituting Eq. (79) into Eqs. (51)–(53), the relationship between the time- and locally

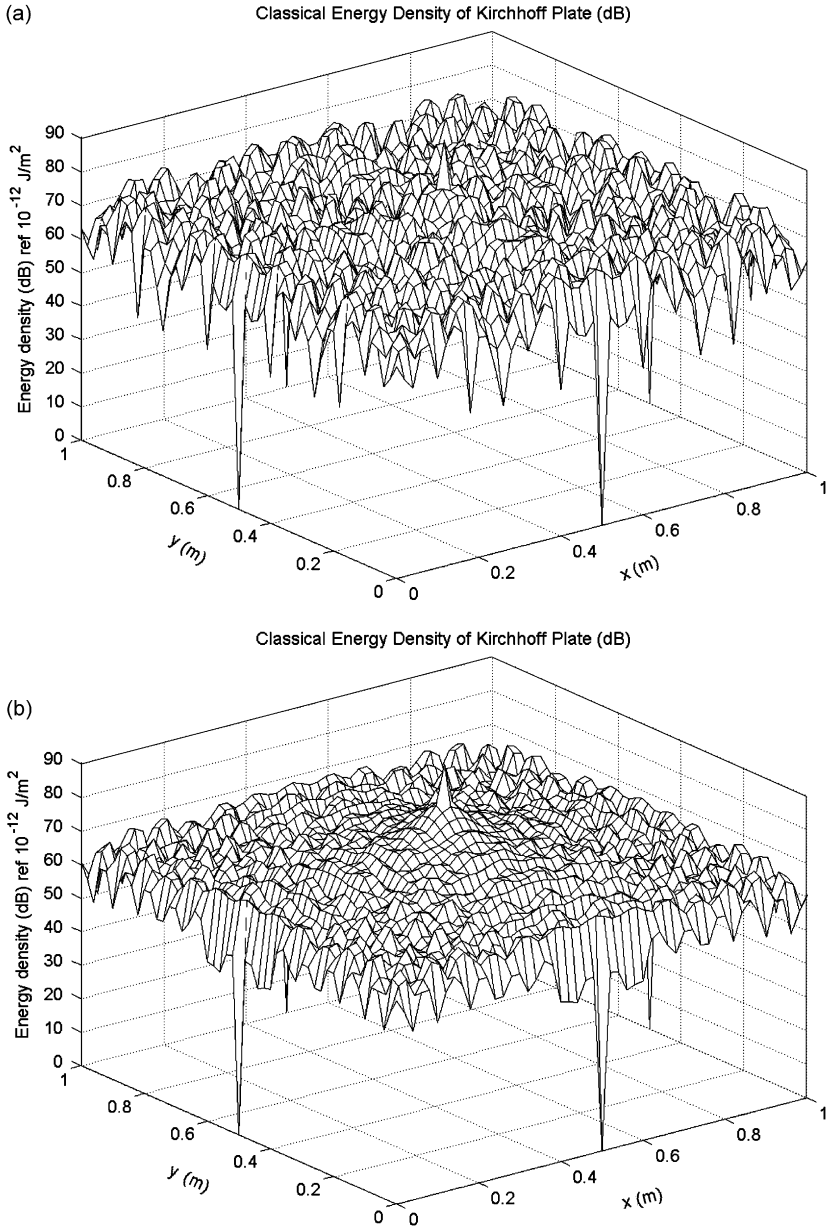

Fig. 7. The energy density level distributions of classical solutions of the Kirchhoff plate ($h = 0.001$ m, $f_c = 1.56$ MHz) when $f = 1$ kHz. The reference energy density is 10^{-12} J/m^2: (a) $\eta = 0.01$, (b) $\eta = 0.1$.

space-averaged far-field smooth energy density and intensity of BDFW is derived by

$$\langle \bar{\mathrm{I}}_2 \rangle = -\frac{c_{g2}^2}{\eta\omega}\left(\frac{\partial}{\partial x}\vec{i}+\frac{\partial}{\partial y}\vec{j}\right)\langle \bar{e}_2 \rangle. \tag{81}$$

By Eqs. (74), (75) and (81), below the critical frequency, the energy governing equation for BDFW is obtained by

$$-\frac{c_{g2}^2}{\eta\omega}\left(\frac{\partial^2}{\partial x^2}+\frac{\partial^2}{\partial y^2}\right)\langle \bar{e}_2 \rangle + \eta\omega\langle \bar{e}_2 \rangle = \pi_{2,\mathrm{in}}. \tag{82}$$

Below the critical frequency, the energetics of BDFW in Eq. (82) is very analogous to that of the flexural wave in the Kirchhoff plate.

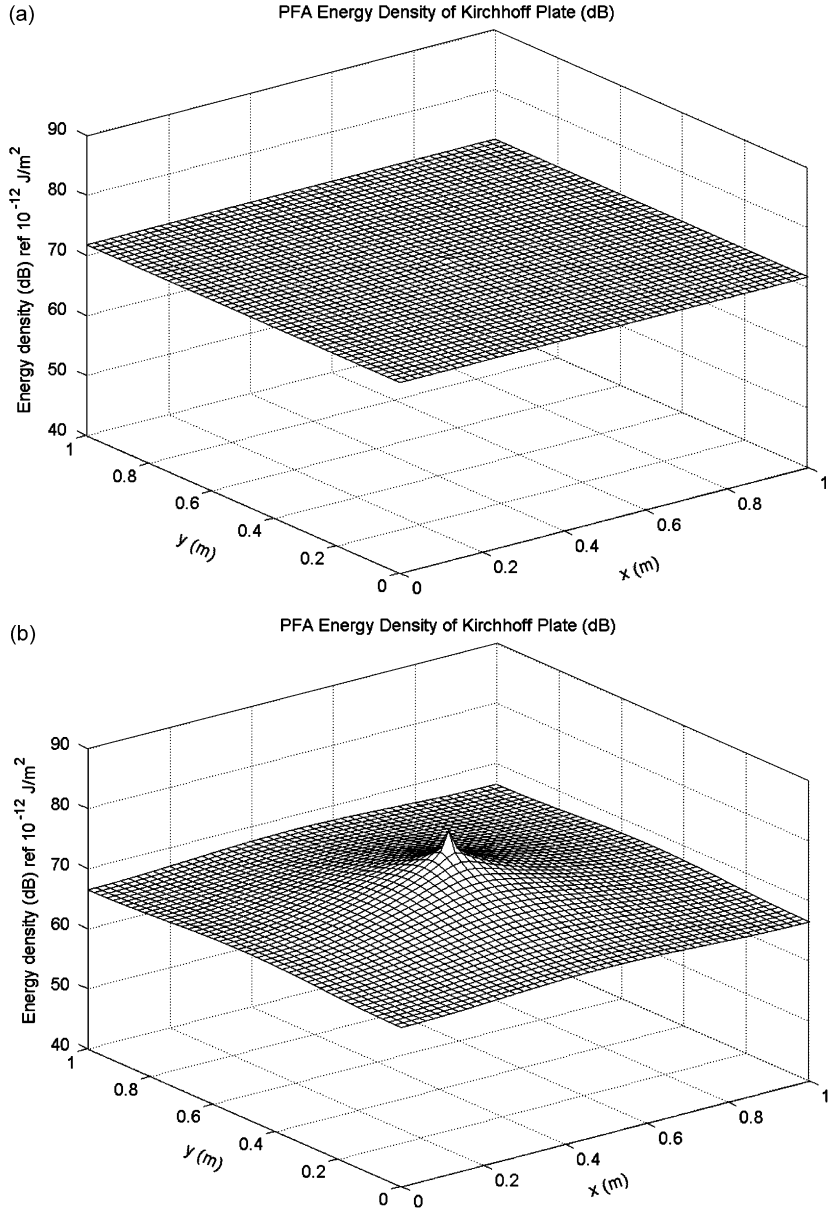

Fig. 8. The energy density level distributions of power flow solutions of the Kirchhoff plate ($h = 0.001$ m, $f_c = 1.56$ MHz) when $f = 1$ kHz. The reference energy density is 10^{-12} J/m^2: (a) $\eta = 0.01$, (b) $\eta = 0.1$.

6. Power flow analysis of a rectangular Mindlin plate

6.1. Power flow solutions for out-of-plane waves in the Mindlin plate

To verify the derived power flow models for out-of-plane waves in the Mindlin plate, numerical analyses were performed for the finite Mindlin plate simply supported along its edges and excited by a transverse harmonic point force as shown in Fig. 4.

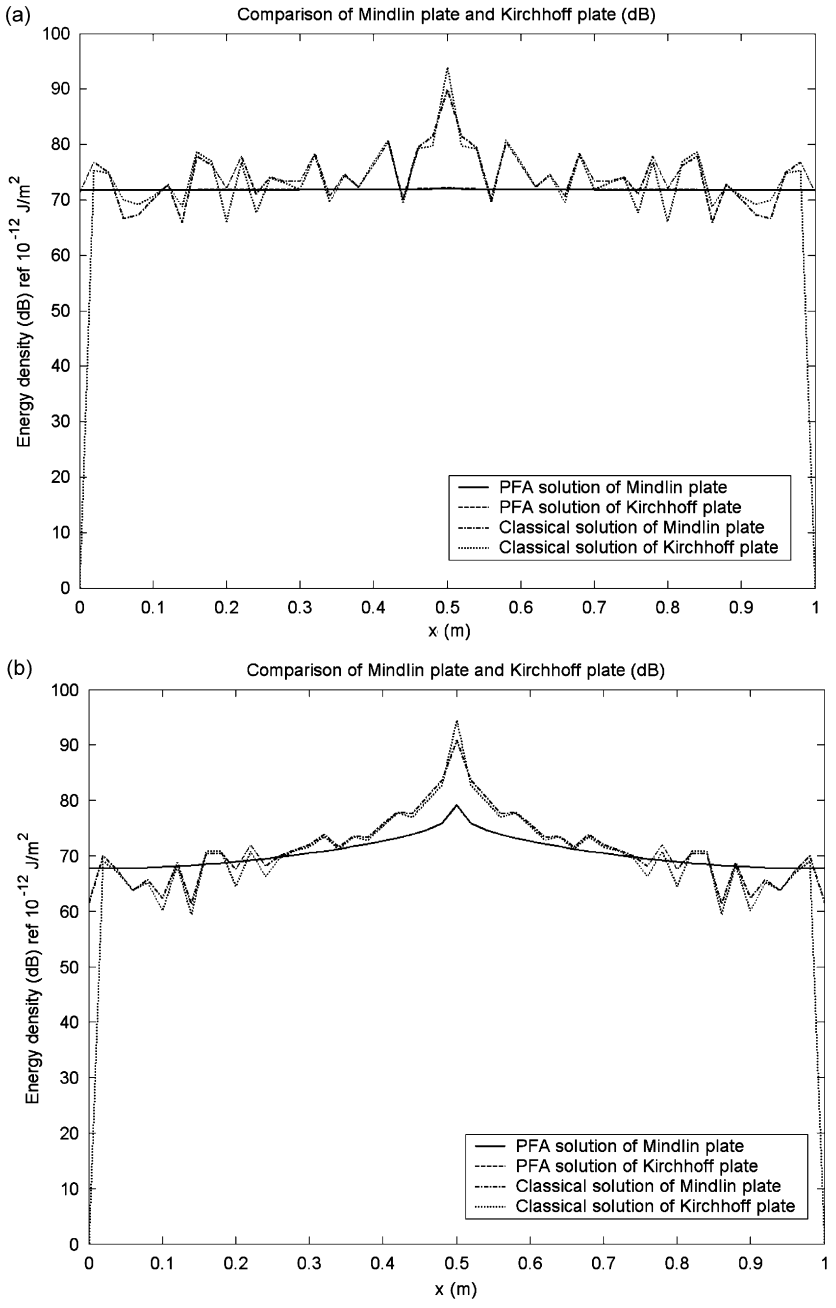

Fig. 9. The comparison of the energy density distributions along the line $y = L_y/2$ of the plate ($h = 0.001$ m, $f_c = 1.56$ MHz) when $f = 1$ kHz. The reference energy density is 10^{-12} J/m^2: (a) $\eta = 0.01$, (b) $\eta = 0.1$: ——, PFA solution of the Mindlin plate; - - - -, PFA solution of the Kirchhoff plate; - · - · -, classical solution of the Mindlin plate; ·····, classical solution of the Kirchhoff plate.

When a point force is excited at (x_0,y_0) of the plate, the energy governing equations for out-of-plane waves (OPSW, BDFW and SDFW) in Eqs. (76)–(78) are expressed by

$$-\frac{c_{gi}^2}{\eta\omega}\left(\frac{\partial^2}{\partial x^2}+\frac{\partial^2}{\partial y^2}\right)\langle\bar{e}_i\rangle+\eta\omega\langle\bar{e}_i\rangle=\pi_{i,in}\delta(x-x_0)\delta(y-y_0)\quad(i=1,2,3). \tag{83}$$

Because there is no power outflow from the simply supported boundary, the energy density solutions (Navier solutions) of Eq. (83) can be expressed by the double Fourier series of the cosine functions with

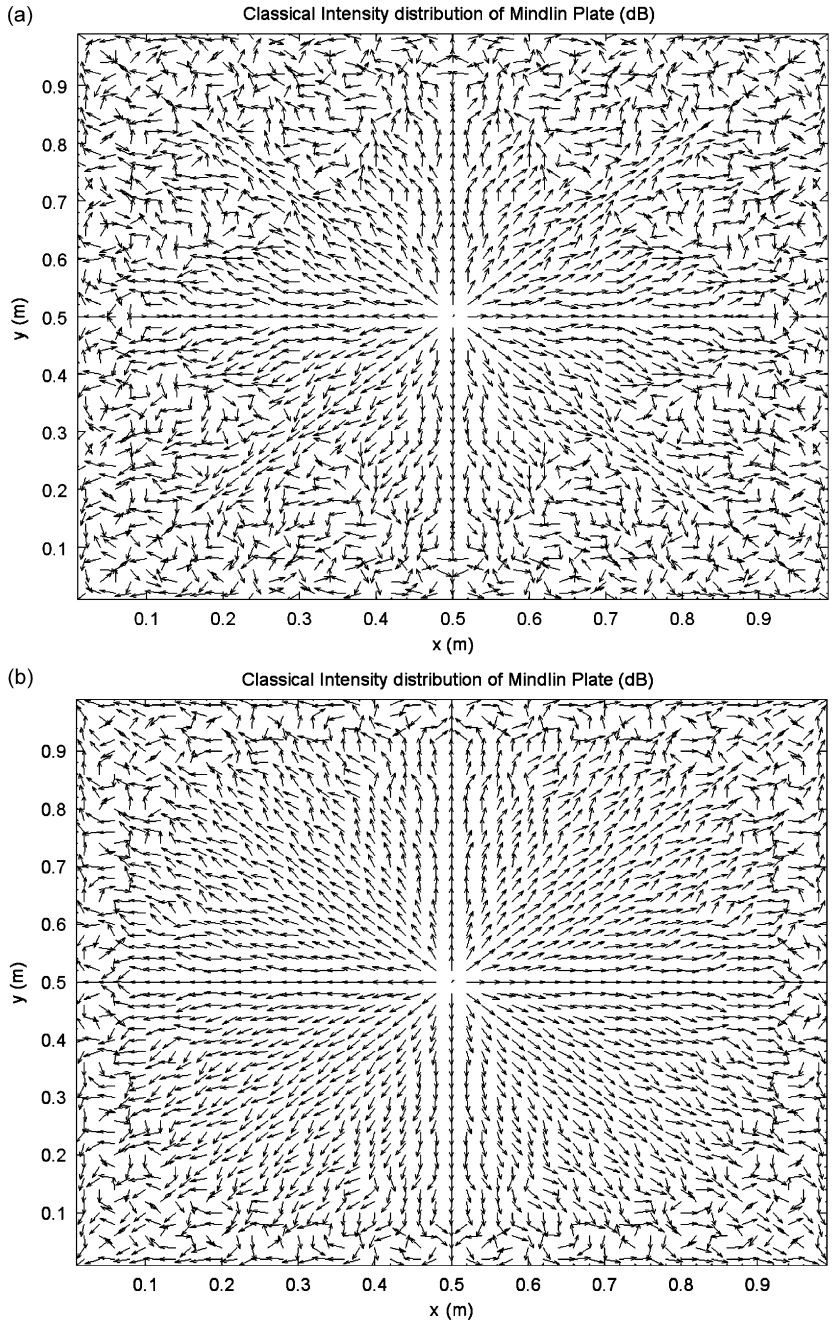

Fig. 10. The intensity level distributions of classical solutions of the Mindlin plate ($h=0.001$ m, $f_c=1.56$ MHz) when $f=1$ kHz. The reference intensity is 10^{-12} W/m^2: (a) $\eta=0.01$, (b) $\eta=0.1$.

respect to the spatial variables x and y, respectively [13]:

$$\langle \bar{e}_i \rangle(x,y) = \sum_{m=0}^{\infty}\sum_{n=0}^{\infty} E_{i,mn} \cos\left(\frac{m\pi x}{L_x}\right)\cos\left(\frac{n\pi y}{L_y}\right) \quad (i=1,2,3), \tag{84}$$

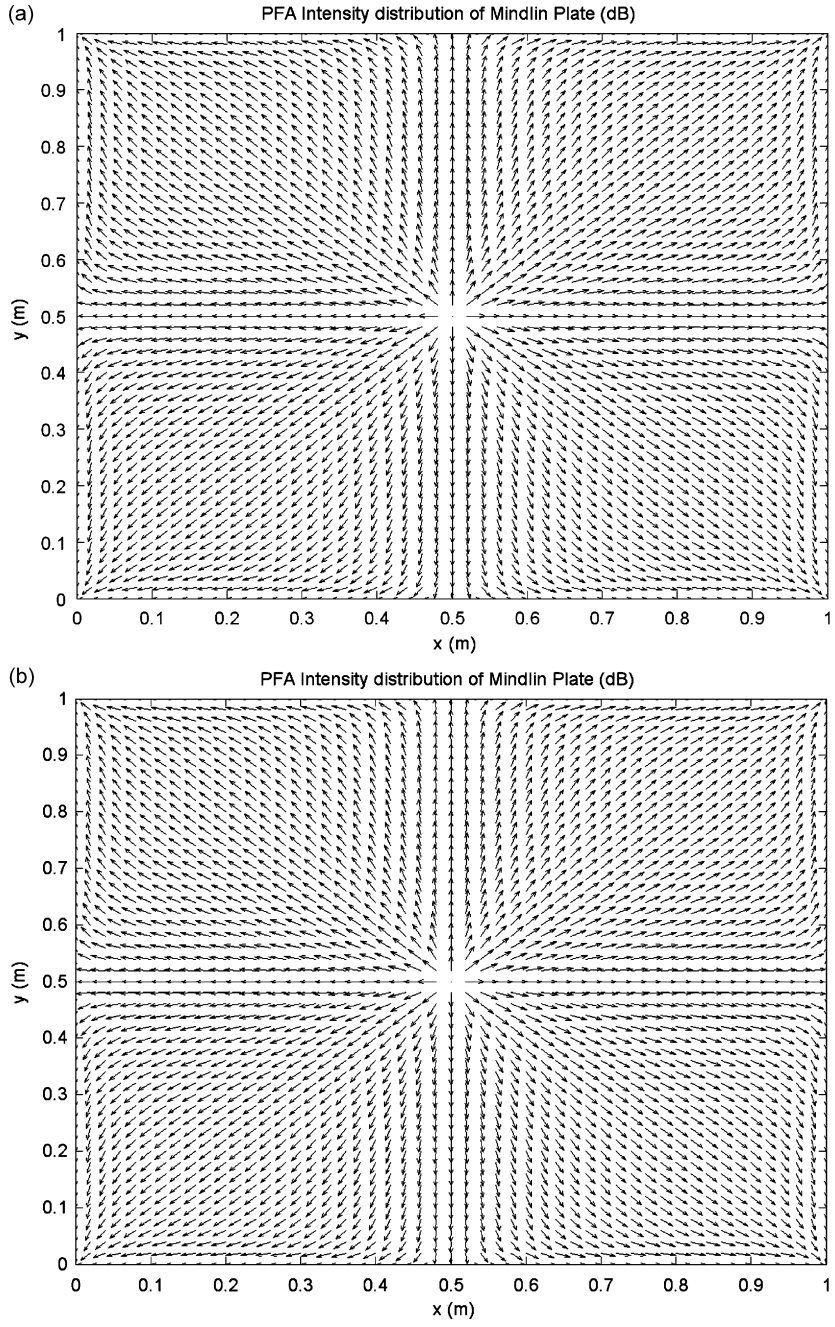

Fig. 11. The intensity level distributions of power flow solutions of the Mindlin plate ($h = 0.001$ m, $f_c = 1.56$ MHz) when $f = 1$ kHz. The reference intensity is 10^{-12} W/m^2: (a) $\eta = 0.01$, (b) $\eta = 0.1$.

where $E_{i,mn}$ is the coefficient of (m,n) mode of the energy density $\langle \bar{e}_i \rangle$, L_x and L_y are the dimensions of the plate as shown in Fig. 4, and "1", "2" and "3" in the subscripts denote OPSW, BDFW and SDFW, respectively.

$$\pi_{i,\mathrm{in}}\delta(x-x_0)\delta(y-y_0) = \sum_{m=0}^{\infty}\sum_{n=0}^{\infty} \Pi_{i,mn} \cos\left(\frac{m\pi x}{L_x}\right)\cos\left(\frac{n\pi y}{L_y}\right) \quad (i=1,2,3), \tag{85}$$

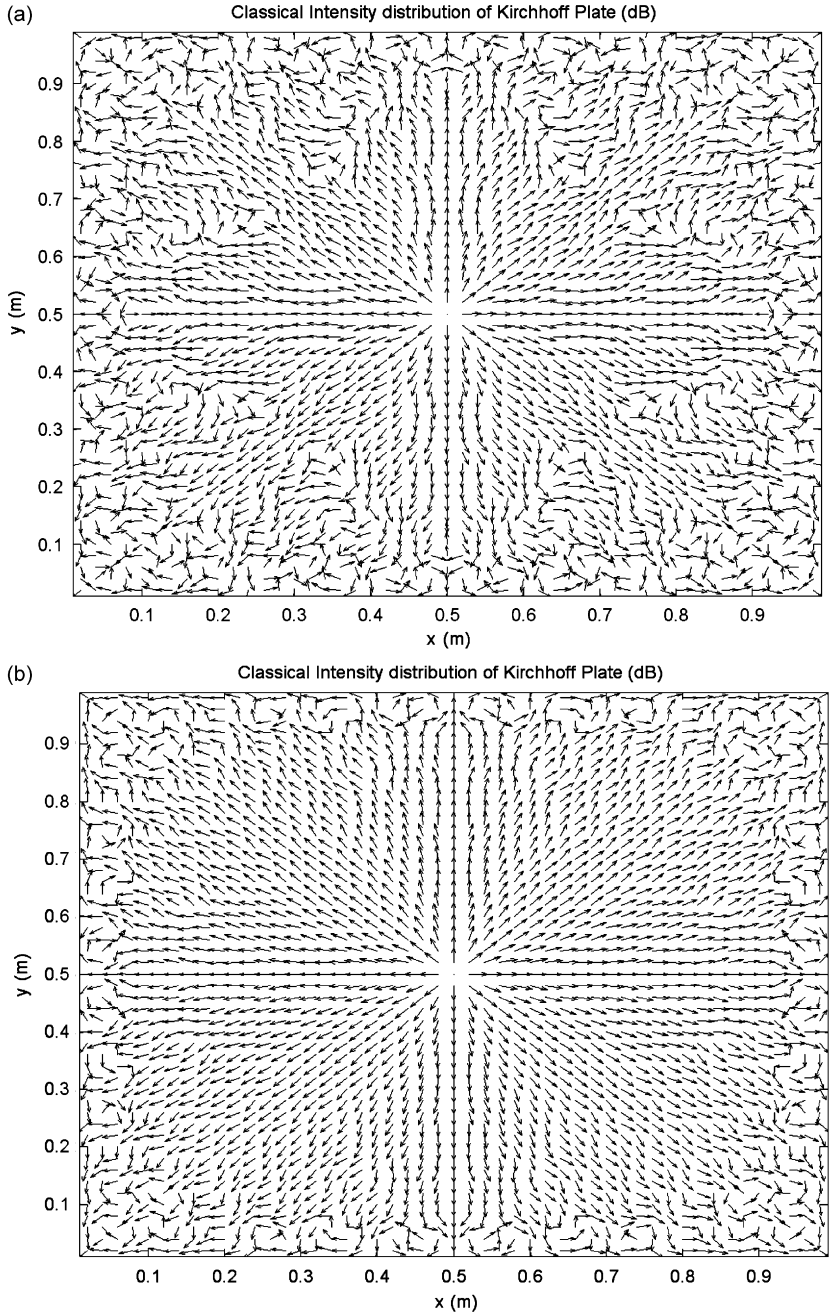

Fig. 12. The intensity level distributions of classical solutions of the Kirchhoff plate ($h = 0.001\,\mathrm{m}$, $f_c = 1.56\,\mathrm{MHz}$) when $f = 1\,\mathrm{kHz}$. The reference intensity is $10^{-12}\,\mathrm{W/m^2}$: (a) $\eta = 0.01$, (b) $\eta = 0.1$.

where the power coefficient of (m,n) mode, $\Pi_{i,mn}$ is

$$\Pi_{i,mn} = \frac{\zeta_{i,mn}}{L_x L_y} \pi_{i,mn} \cos\left(\frac{m\pi x_0}{L_x}\right) \cos\left(\frac{n\pi y_0}{L_y}\right) \quad (i = 1, 2, 3), \tag{86}$$

where

$$\zeta_{i,mn} = \begin{cases} 1, & m = 0 \text{ and } n = 0 \\ 2, & (m \neq 0 \text{ and } n = 0) \quad \text{or} \quad (m = 0 \text{ and } n \neq 0) \\ 4, & m \neq 0 \text{ and } n \neq 0 \end{cases}. \tag{87}$$

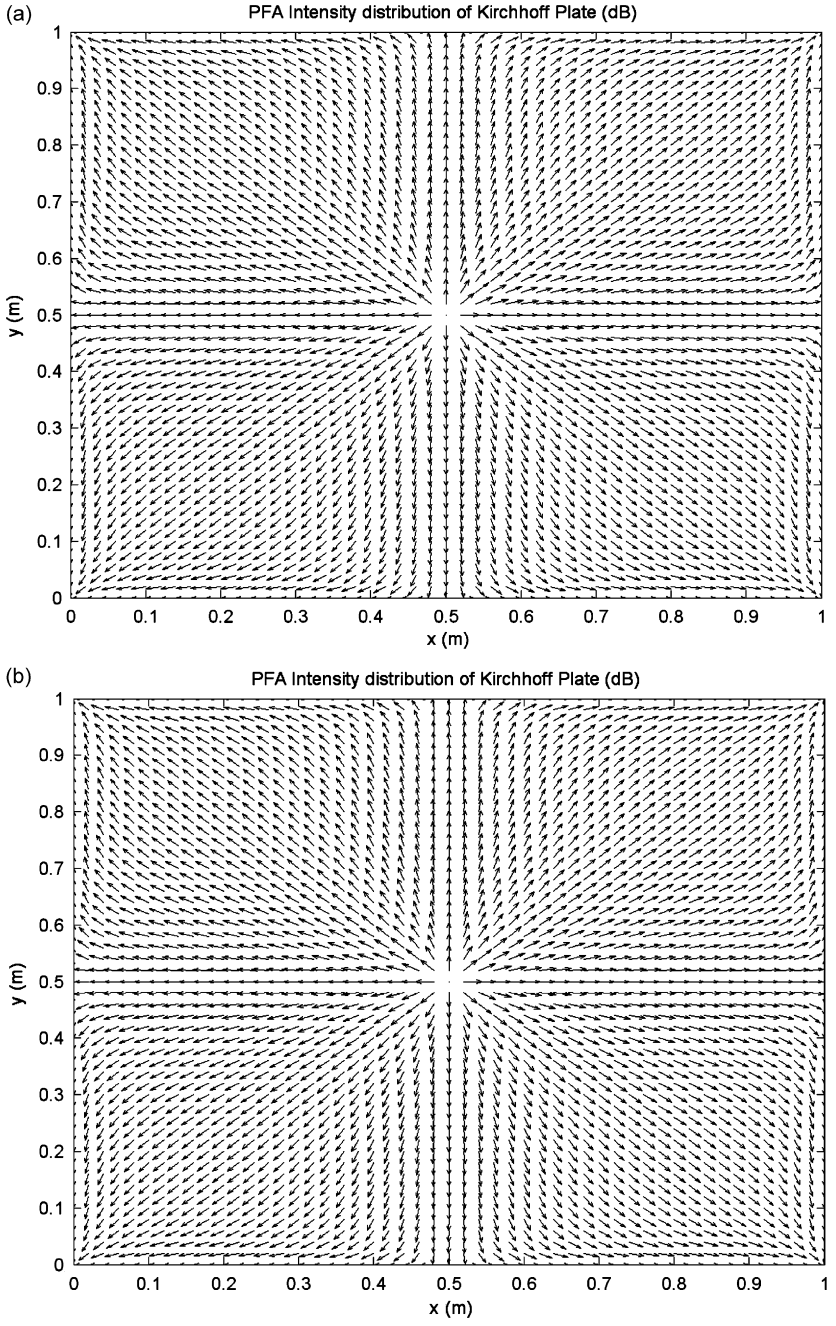

Fig. 13. The intensity level distributions of power flow solutions of the Kirchhoff plate ($h = 0.001$ m, $f_c = 1.56$ MHz) when $f = 1$ kHz. The reference intensity is 10^{-12} W/m^2: (a) $\eta = 0.01$, (b) $\eta = 0.1$.

Substituting Eqs. (84)–(86) into Eq. (83), the modal participation factors of energy densities are represented as

$$E_{i,mn} = \frac{(\zeta_{i,mn}/L_xL_y)\pi_{i,\mathrm{in}}\cos(m\pi x_0/L_x)\cos(n\pi y_0/L_y)}{(c_{gi}^2/\eta\omega)\{(m\pi/L_x)^2+(n\pi/L_y)^2\}+\eta\omega} \quad (i=1,2,3). \tag{88}$$

By Eqs. (54) and (55), the time- and locally space-averaged total far-field smooth energy density and intensity solutions are expressed by, respectively,

$$\langle \bar{e} \rangle = \sum_{i=1}^{3}\left[\sum_{m=0}^{\infty}\sum_{n=0}^{\infty} E_{i,mn}\cos\left(\frac{m\pi x}{L_x}\right)\cos\left(\frac{n\pi y}{L_y}\right)\right], \tag{89}$$

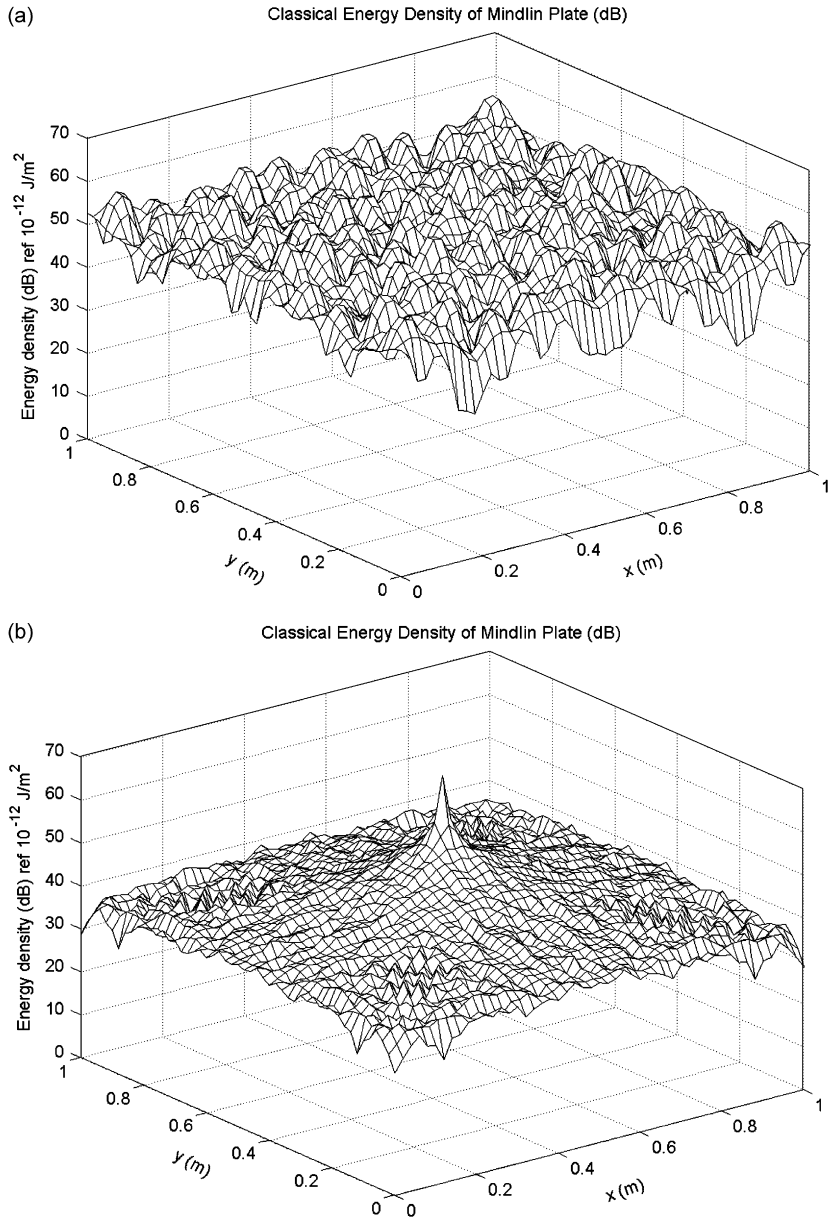

Fig. 14. The energy density level distributions of classical solutions of the Mindlin plate ($h = 0.01\,\mathrm{m}$, $f_c = 156\,\mathrm{kHz}$) when $\eta = 0.01$. The reference energy density is $10^{-12}\,\mathrm{J/m^2}$: (a) $f = 5\,\mathrm{kHz}$, (b) $f = 200\,\mathrm{kHz}$.

and

$$\langle \bar{\mathrm{I}} \rangle = \left[\sum_{i=1}^{3} \left\{ \frac{c_{gi}^2}{\eta\omega} \sum_{m=0}^{\infty} \sum_{n=0}^{\infty} E_{i,mn} \left(\frac{m\pi}{L_x} \right) \sin\left(\frac{m\pi x}{L_x} \right) \cos\left(\frac{n\pi y}{L_y} \right) \right\} \right] \vec{i} + \left[\sum_{i=1}^{3} \left\{ \frac{c_{gi}^2}{\eta\omega} \sum_{m=0}^{\infty} \sum_{n=0}^{\infty} E_{i,mn} \left(\frac{n\pi}{L_y} \right) \cos\left(\frac{m\pi x}{L_x} \right) \sin\left(\frac{n\pi y}{L_y} \right) \right\} \right] \vec{j}. \tag{90}$$

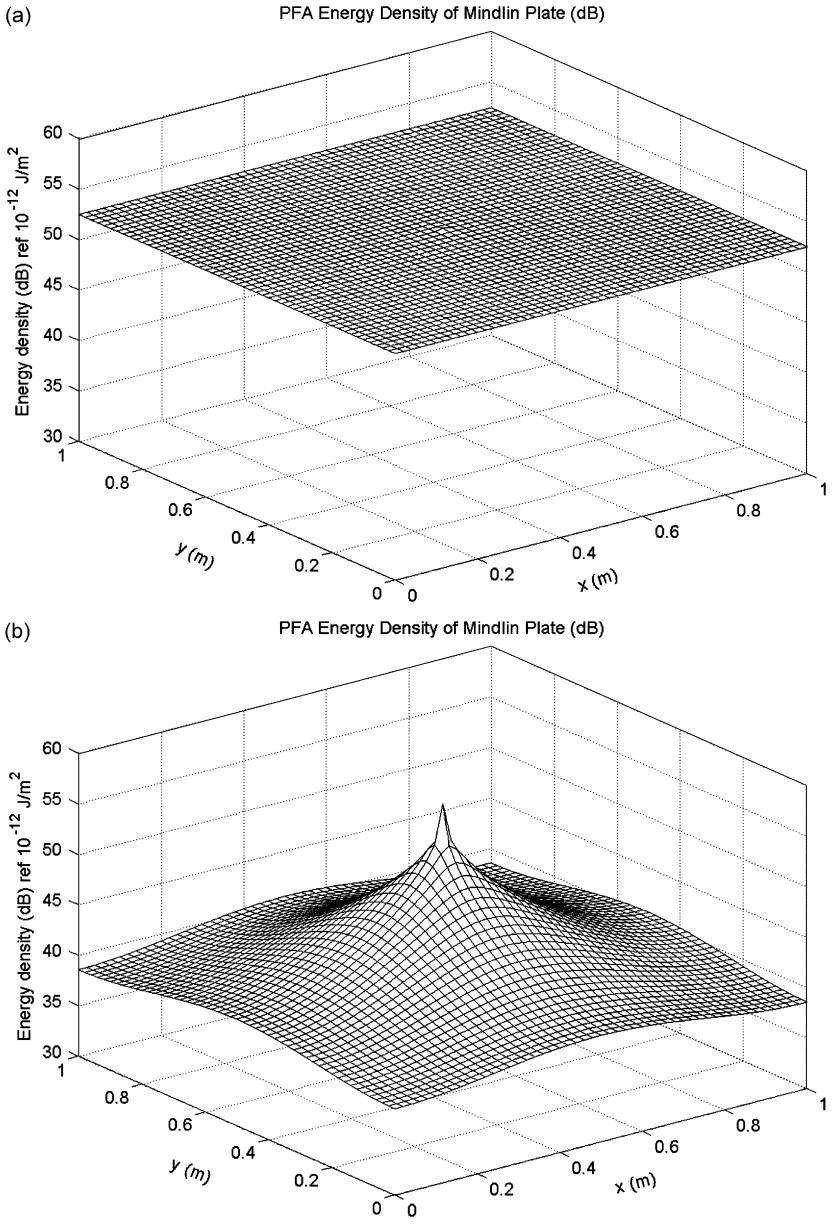

Fig. 15. The energy density level distributions of power flow solutions of the Mindlin plate ($h = 0.01\,\mathrm{m}$, $f_c = 156\,\mathrm{kHz}$) when $\eta = 0.01$. The reference energy density is $10^{-12}\,\mathrm{J/m^2}$: (a) $f = 5\,\mathrm{kHz}$, (b) $f = 200\,\mathrm{kHz}$.

6.2. Numerical examples

Numerical analyses were performed for a finite rectangular isotropic plate simply supported along its edges and excited by a transverse harmonic point force. The energy density and intensity distributions obtained by the developed power flow models for the Mindlin plate were compared with the results obtained by the classical solutions for the Mindlin plate (Appendix B), and with the classical solutions and the power flow solutions for the Kirchhoff plate [20], respectively. In the first example, the dimensions of a plate were $L_x \times L_y \times h = 1\,\text{m} \times 1\,\text{m} \times 0.001\,\text{m}$, as shown in Fig. 4, and the material properties of a plate were assumed to be the same as those of steel. The critical frequency of this plate was about $f_c = 1.56\,\text{MHz}$. The external point force was located at $x_0 = L_x/2$ and $y_0 = L_y/2$ in the plate and its amplitude was $F = 1\,\text{N}$. According to

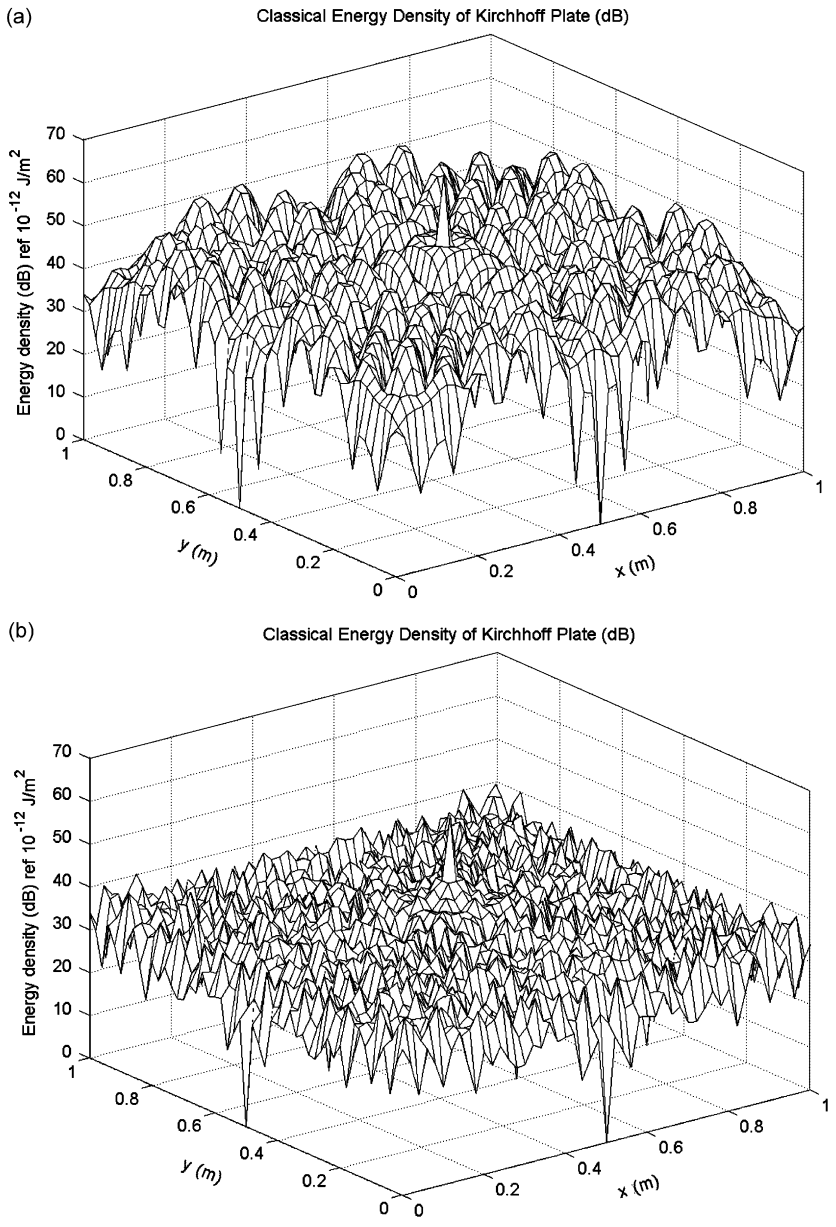

Fig. 16. The energy density level distributions of classical solutions of the Kirchhoff plate ($h = 0.01\,\text{m}$, $f_c = 156\,\text{kHz}$) when $\eta = 0.01$. The reference energy density is $10^{-12}\,\text{J/m}^2$: (a) $f = 5\,\text{kHz}$, (b) $f = 200\,\text{kHz}$.

excitation frequency, the time-averaged input power used to obtain the power flow solution was calculated as follows:

$$\pi_{\text{in}} = \frac{1}{2}\text{Re}\left\{(F e^{j\omega t}) \times \left(\frac{\partial w(x_0, y_0, t)}{\partial t}\right)^*\right\} = \begin{array}{ll} \pi_{1,\text{in}} & (\omega \leqslant \omega_c) \\ \pi_{1,\text{in}} + \pi_{2,\text{in}} + \pi_{3,\text{in}} & (\omega > \omega_c) \end{array}, \tag{91}$$

where $\partial w/\partial t$ was obtained by the classical solution expressed as Eq. (B.10).

For excitation frequency of 1 kHz, the spatial distributions of the energy density and intensity obtained by each solution for various values of hysteretic damping ($\eta = 0.01$, $\eta = 0.1$) are shown in Figs. 5 and 6. For the sufficient accuracy of Navier solutions, 25,000 lower modal terms of the series were used to obtain the classical and PFA results, respectively. Generally, to guarantee the sufficient convergence, the Navier solutions for the

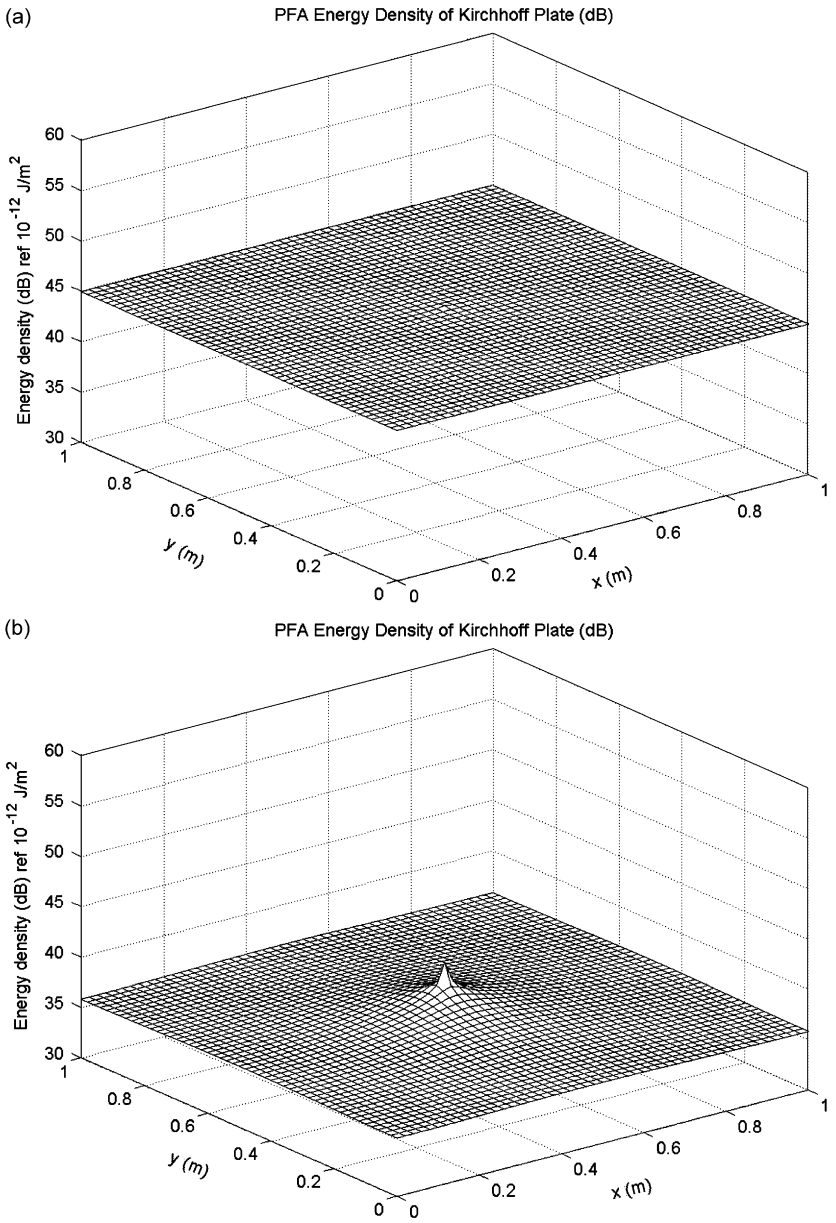

Fig. 17. The energy density level distributions of power flow solutions of the Kirchhoff plate ($h = 0.01$ m, $f_c = 156$ kHz) when $\eta = 0.01$. The reference energy density is 10^{-12} J/m^2: (a) $f = 5$ kHz, (b) $f = 200$ kHz.

Mindlin plate model need much more modal terms than those for the Kirchhoff plate model. In Figs. 5 and 6, the developed PFA solutions for the Mindlin plate represent well the global variation of the classical solutions for the Mindlin plate like the cases of the Kirchhoff plate shown in Figs. 7 and 8, regardless of the hysteretic damping of the plate. These results can be clearly observed in Fig. 9, which shows energy densities of each solution along the line $x = L_x/2$. In results by both plate models, as the hysteretic damping of the plate increases, the global variations of energy densities predicted by the classical and PFA solutions increase, as

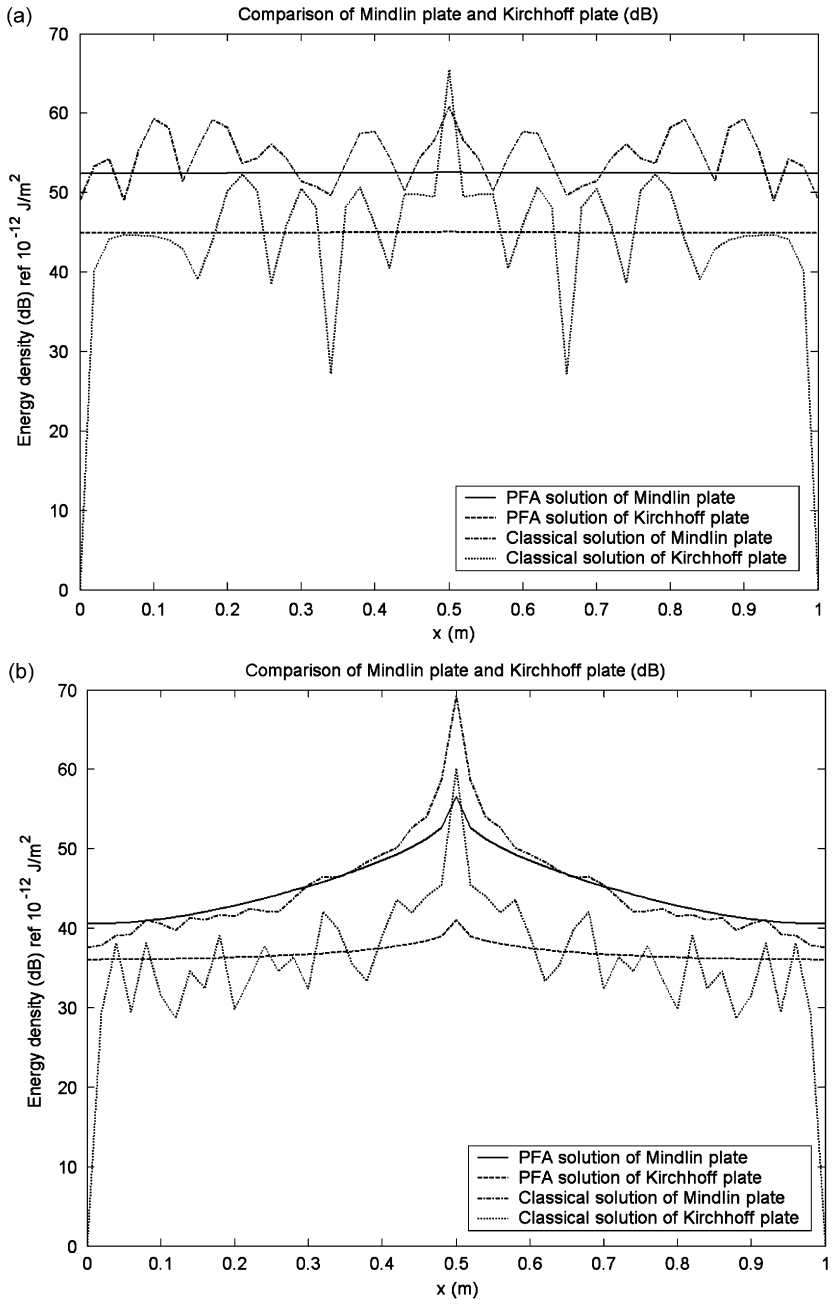

Fig. 18. The comparison of the energy density distributions along the line $y = L_y/2$ of the plate ($h = 0.01$ m, $f_c = 156$ kHz) when $\eta = 0.01$. The reference energy density is 10^{-12} J/m^2: (a) $f = 5$ kHz, (b) $f = 200$ kHz: ——, PFA solution of the Mindlin plate; - - - -, PFA solution of the Kirchhoff plate; - · - · -, classical solution of the Mindlin plate; ·····, classical solution of the Kirchhoff plate.

seen in Figs. 5–8, and the spatial distributions of energy densities predicted by the classical solution and the PFA solution become more similar due to the increase of modal overlap in the classical solution except the vicinity of the driving point where the direct field is dominant. Additionally, because the excitation frequency (1 kHz) is much lower than the critical frequency ($f_c = 1.56$ MHz) of a plate, the effects of shear distortion and rotatory inertia are not dominant over the effect of bending. Therefore, as shown in Fig. 9, the results obtained by the Mindlin plate model are almost equivalent to those by the Kirchhoff plate model. Figs. 10 and 11 show the intensity distributions predicted by the classical solution and PFA solution for the Mindlin plate model, respectively. Figs. 12 and 13 show the intensity distributions predicted by the classical solution and PFA solution for the Kirchhoff plate model, respectively. Like the previous case of energy density, the spatial intensity distributions of the classical solution and the PFA solution for each plate model become more similar

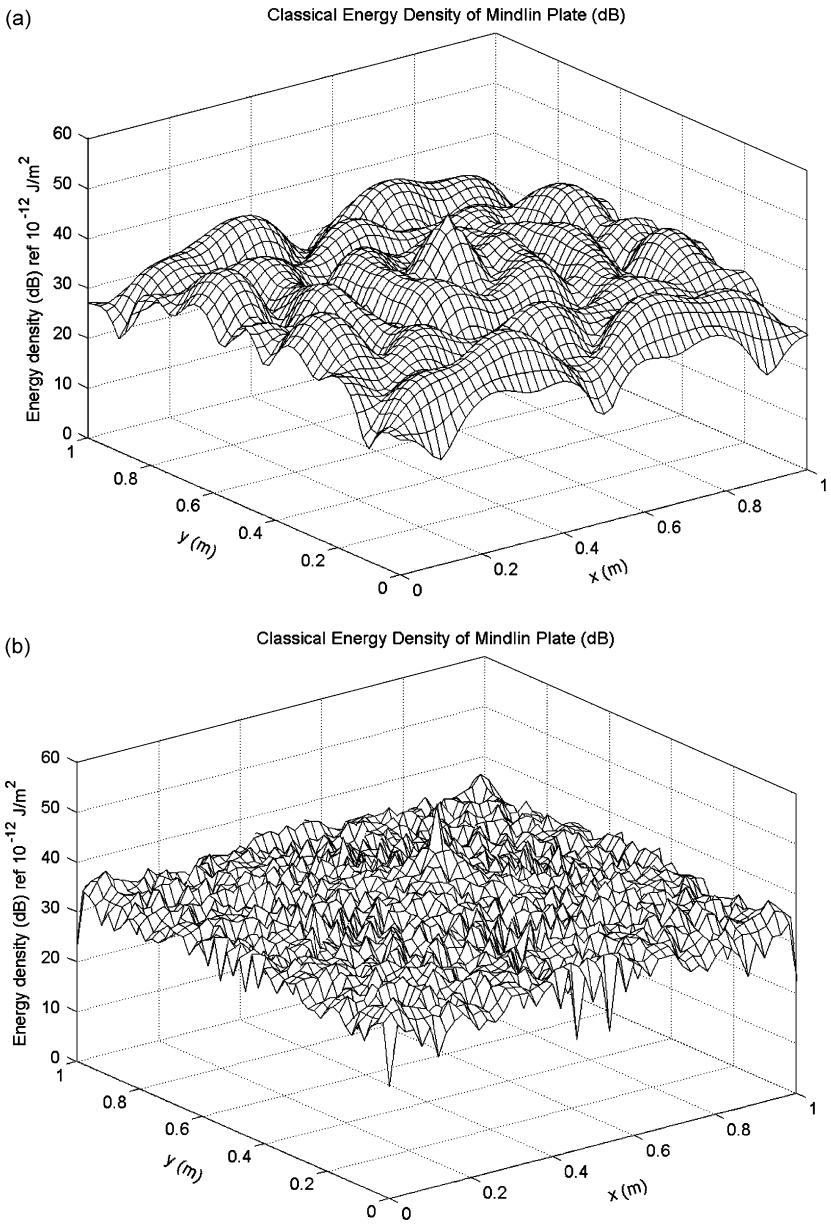

Fig. 19. The energy density level distributions of classical solutions of the Mindlin plate ($h = 0.04$ m, $f_c = 39.1$ kHz) when $\eta = 0.01$. The reference energy density is 10^{-12} J/m^2: (a) $f = 4$ kHz, (b) $f = 70$ kHz.

as the hysteretic damping increases, and the spatial intensity distributions obtained by the Mindlin and Kirchhoff plate models are almost identical because of low excitation frequency, as shown in Figs. 10–13.

For the next examples, the thickness and hysteretic damping of the plate were set to be $h = 0.01\,m$ and $\eta = 0.01$, respectively. The critical frequency of this plate was about 156 kHz. In Figs. 14 and 15, the developed PFA solutions for the Mindlin plate represent well the global variation of the classical solutions for the Mindlin plate like the cases of the Kirchhoff plate shown in Figs. 16 and 17, regardless of the excitation frequency. In results by both plate models, as the excitation frequency increases, the energy density decreases fast with increasing distance from the driving point. In Fig. 18(a), though the excitation frequency is lower than the critical frequency, the energy density distributions obtained by the classical and PFA solutions for the Mindlin plate differ from those obtained by those for the Kirchhoff plate because the effects of shear

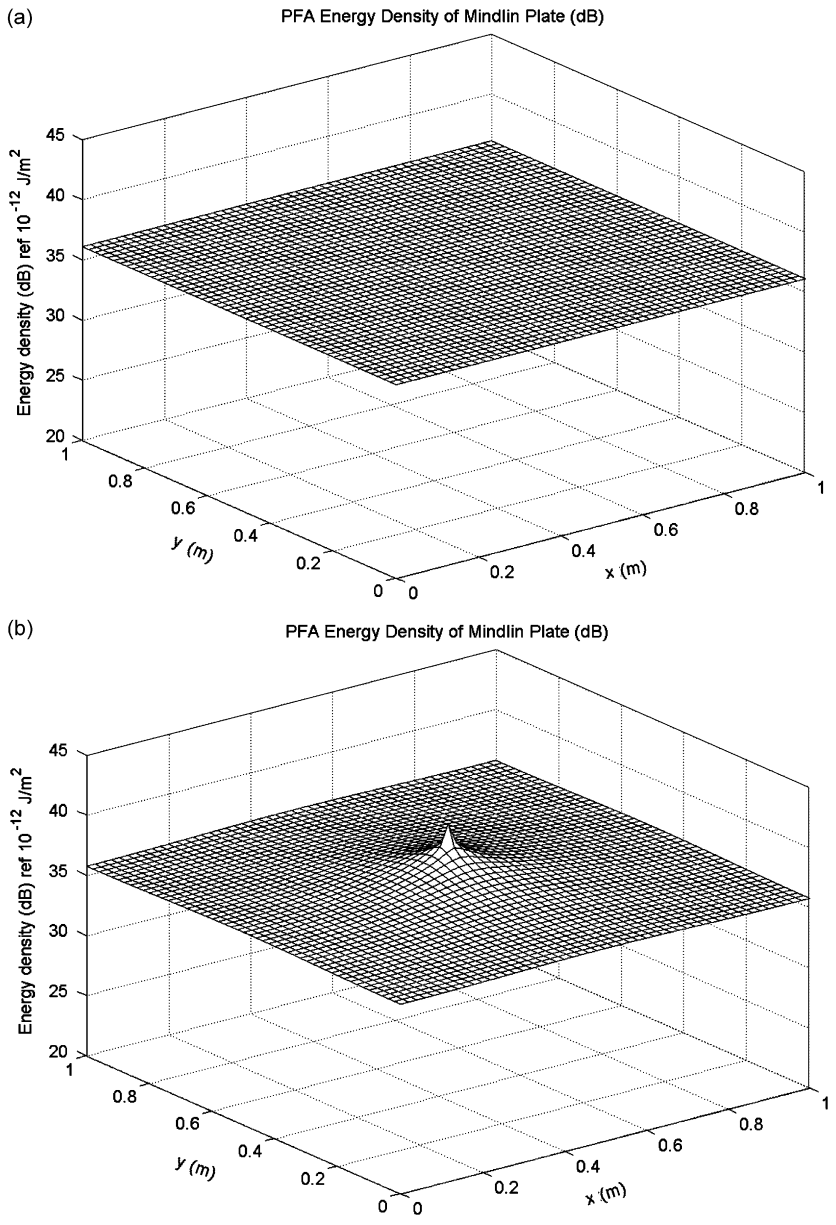

Fig. 20. The energy density level distributions of power flow solutions of the Mindlin plate ($h = 0.04\,\text{m}$, $f_c = 39.1\,\text{kHz}$) when $\eta = 0.01$. The reference energy density is $10^{-12}\,\text{J/m}^2$: (a) $f = 4\,\text{kHz}$, (b) $f = 70\,\text{kHz}$.

distortion and rotatory inertia are not ignorable. When the excitation frequency is higher than the critical frequency, because the effects of shear distortion and rotatory inertia are dominant, the differences of spatial energy distributions as well as energy levels predicted by the Mindlin and Kirchhoff plate models are more prominent as shown in Fig. 18(b).

In the last examples, only the thickness of the plate in the second example is changed to $h = 0.04\,\mathrm{m}$. This plate model has the critical frequency of $f_c = 39.1\,\mathrm{kHz}$, which is relatively lower than the critical frequencies of previous examples. Therefore, the effects of shear distortion and rotatory inertia become more important at low frequencies in this example than in previous examples. Figs. 19 and 20 show the effects of shear distortion and rotatory inertia are dominant even at low frequencies and the energy model for the Mindlin plate is derived successfully (see Figs. 21 and 22). In Fig. 23, the spatial distributions and levels of energy densities

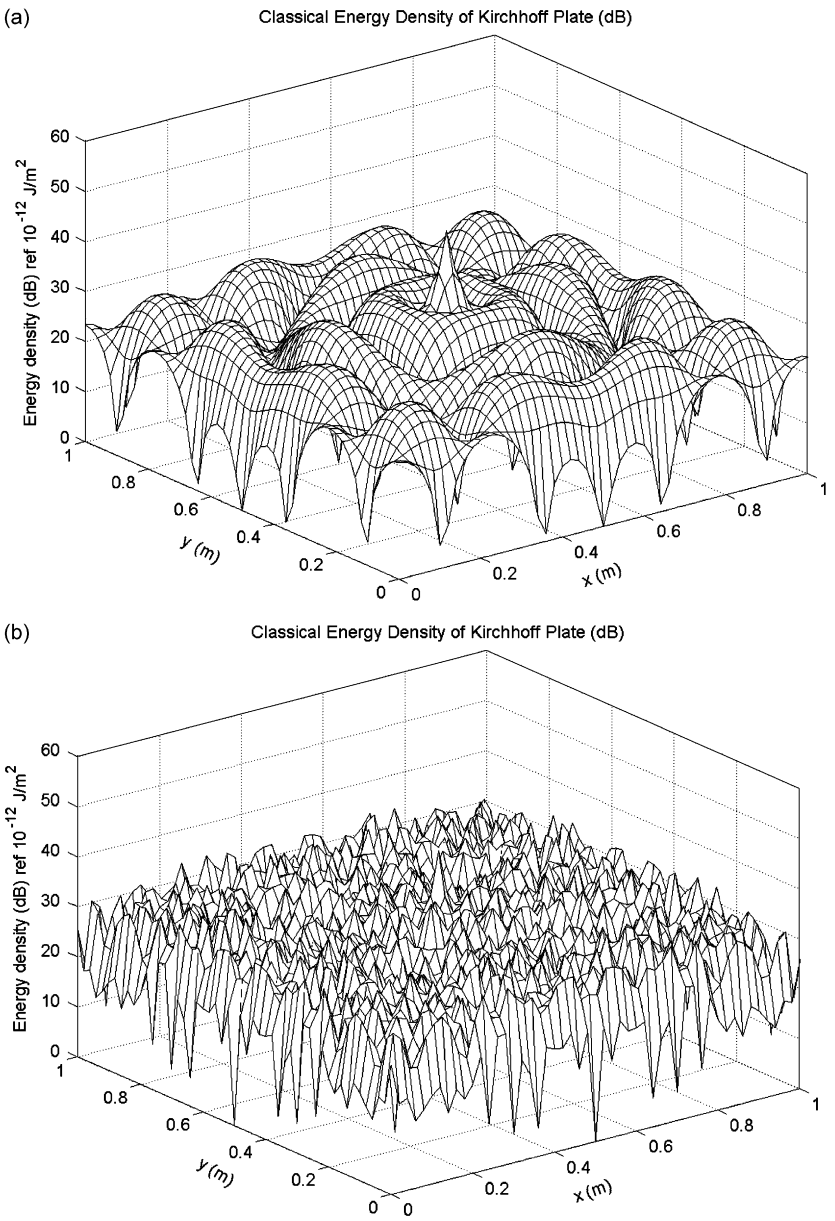

Fig. 21. The energy density level distributions of classical solutions of the Kirchhoff plate ($h = 0.04\,\mathrm{m}$, $f_c = 39.1\,\mathrm{kHz}$) when $\eta = 0.01$. The reference energy density is $10^{-12}\,\mathrm{J/m^2}$: (a) $f = 4\,\mathrm{kHz}$, (b) $f = 70\,\mathrm{kHz}$.

predicted by the Mindlin and Kirchhoff plate models are considerably different at both 4 and 70 kHz, which are lower and higher than the critical frequency, respectively.

7. Conclusion

For the improved vibrational analysis for out-of-plane motions in a two-dimensional plate structure in the medium-to-high-frequency ranges, power flow models were newly developed for propagating out-of-plane waves in a finite Mindlin plate. The derived power flow models have different forms depending on the exciting frequency and are the general energetic model for out-of-plane motion in the plate, incorporating not only the

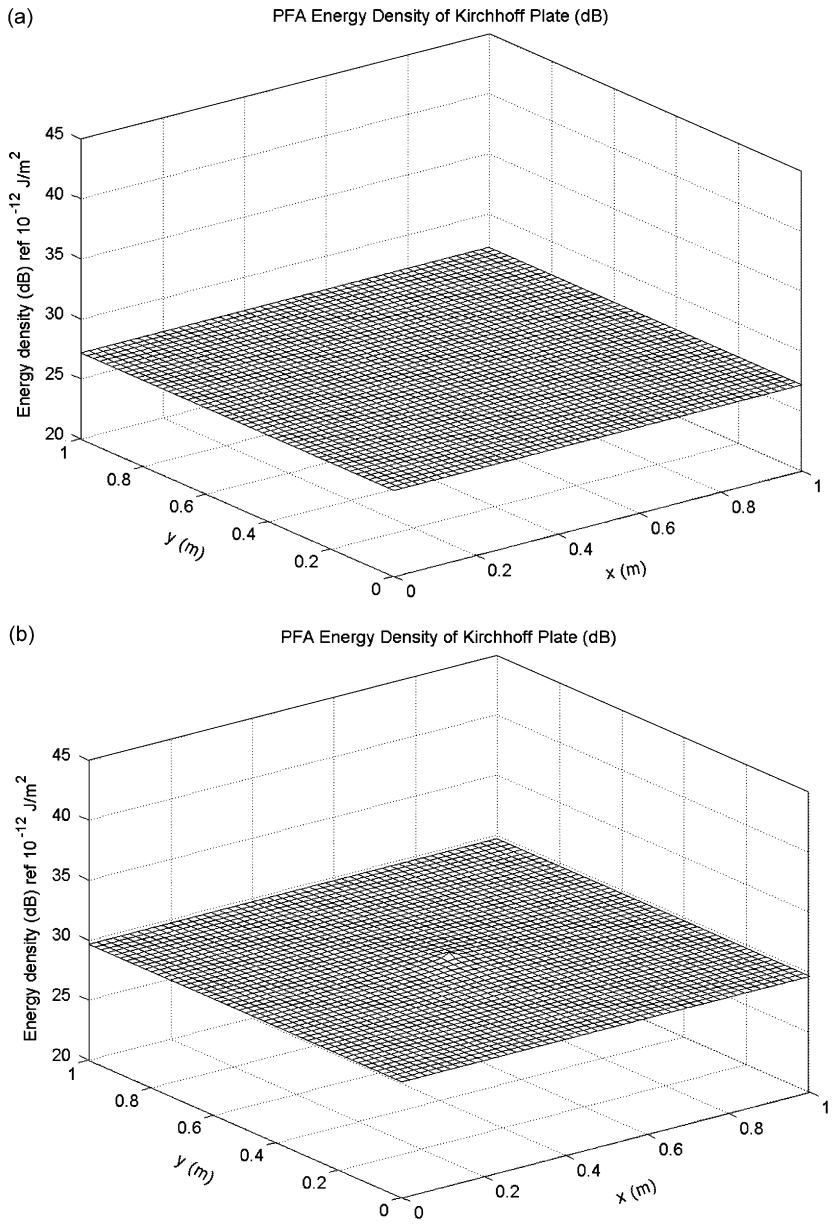

Fig. 22. The energy density level distributions of power flow solutions of the Kirchhoff plate ($h = 0.04$ m, $f_c = 39.1$ kHz) when $\eta = 0.01$. The reference energy density is 10^{-12} J/m^2: (a) $f = 4$ kHz, (b) $f = 70$ kHz.

Kirchhoff plate theory used for the conventional power flow model but also the Mindlin plate theory. Below the critical frequency, the energy governing equation for one propagating out-of-plane wave, BDFW, like that of the Kirchhoff plate is obtained. Above the critical frequency, the energy governing equations for three kinds of propagating out-of-plane waves, OPSW, BDFW, and SDFW, are found.

To verify the developed power flow models, numerical analyses of various examples were performed. As expected, the developed power flow solutions for the Mindlin plate agreed well with the global variation of the

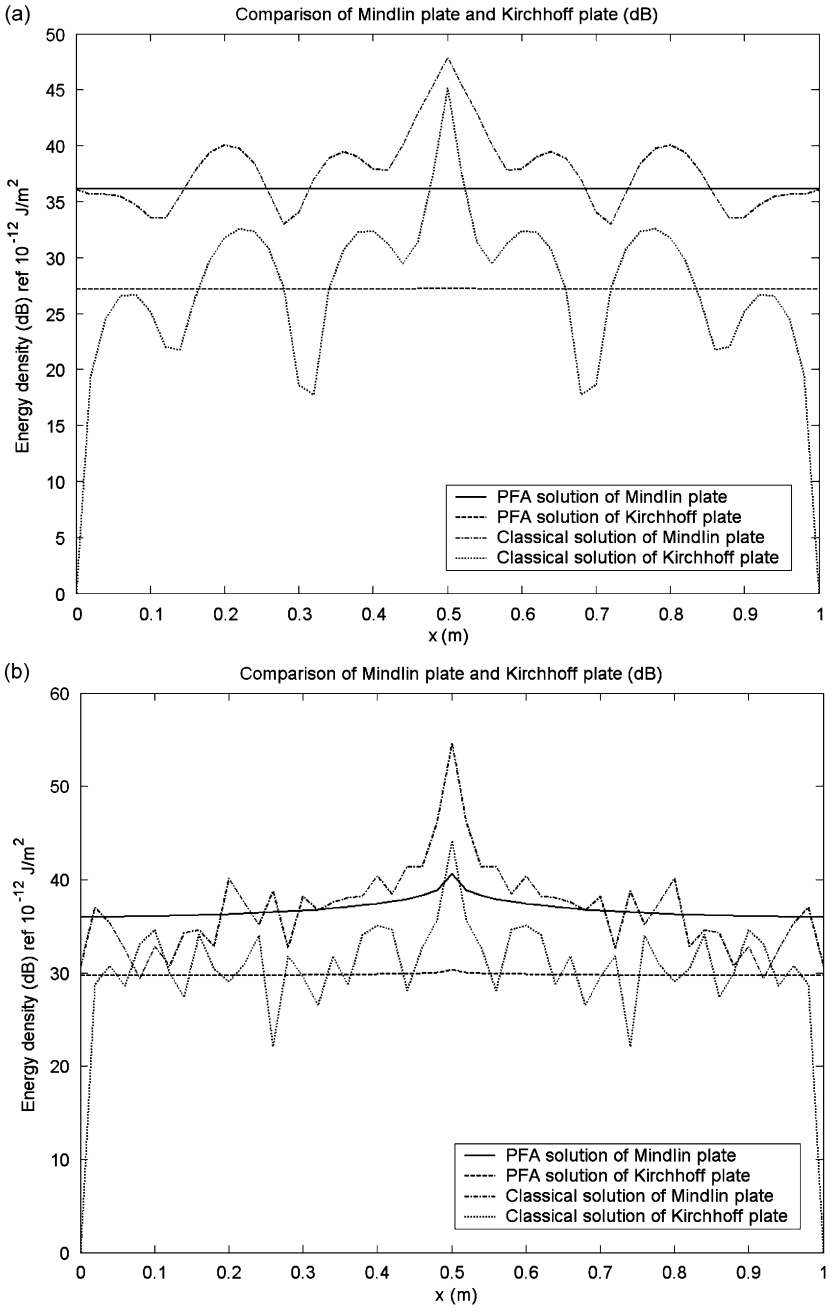

Fig. 23. The comparison of the energy density distributions along the line $y = L_y/2$ of the plate ($h = 0.04\,\text{m}, f_c = 39.1\,\text{kHz}$) when $\eta = 0.01$. The reference energy density is $10^{-12}\,\text{J/m}^2$: (a) $f = 4\,\text{kHz}$, (b) $f = 70\,\text{kHz}$: ——, PFA solution of the Mindlin plate; - - - -, PFA solution of the Kirchhoff plate; - · - · -, classical solution of the Mindlin plate; ·····, classical solution of the Kirchhoff plate.

classical solutions for the Mindlin plate at various excitation frequencies and hysteretic damping factors. Additionally, as the exciting frequency increases and the plate becomes thicker, the developed power flow solutions for the Mindlin plate become greatly different from the traditional power flow solutions for the Kirchhoff plate. Therefore, the developed power flow model for out-of-plane motion in the Mindlin plate can be an improved tool for prediction of diffuse vibrational behavior in a plate at medium-to-high frequencies.

Acknowledgements

This work was partially supported by ASERC (Advanced Ship Engineering Research Center) of the Korea Science & Engineering Foundation and RIMSE (Research Institute of Marine Systems Engineering) of Seoul National University.

Appendix A. Derivation of time- and locally space-averaged far-field smooth energy density and intensity

A.1. Above the critical frequency

Above the critical frequency, all kinds of out-of-plane waves of general solution in Eqs. (31) and (32) are far-field components. The far-field solutions composed of transverse displacement w, displacement potential functions ϕ and ψ by Eqs. (31) and (32), can be rewritten as, respectively,

$$w = \left[\left\{P_1 e^{(-jk_{2cx}x - jk_{2cy}y)} + P_2 e^{(-jk_{2cx}x + jk_{2cy}y)} + P_3 e^{(jk_{2cx}x - jk_{2cy}y)} + P_4 e^{(jk_{2cx}x + jk_{2cy}y)}\right\} + \left\{Q_1 e^{(-jk_{3cx}x - jk_{3cy}y)} + Q_2 e^{(-jk_{3cx}x + jk_{3cy}y)} + Q_3 e^{(jk_{3cx}x - jk_{3cy}y)} + Q_4 e^{(jk_{3cx}x + jk_{3cy}y)}\right\}\right] e^{j\omega t}, \tag{A.1}$$

$$\phi = \left[\left\{R_1 e^{(-jk_{2cx}x - jk_{2cy}y)} + R_2 e^{(-jk_{2cx}x + jk_{2cy}y)} + R_3 e^{(jk_{2cx}x - jk_{2cy}y)} + R_4 e^{(jk_{2cx}x + jk_{2cy}y)}\right\} + \left\{S_1 e^{(-jk_{3cx}x - jk_{3cy}y)} + S_2 e^{(-jk_{3cx}x + jk_{3cy}y)} + S_3 e^{(jk_{3cx}x - jk_{3cy}y)} + S_4 e^{(jk_{3cx}x + jk_{3cy}y)}\right\}\right] e^{j\omega t} \tag{A.2}$$

and

$$\psi = \left\{T_1 e^{(-jk_{1cx}x - jk_{1cy}x)} + T_2 e^{(-jk_{1cx}x + jk_{1cy}x)} + T_3 e^{(jk_{1cx}x - jk_{1cy}x)} + T_4 e^{(jk_{1cx}x + jk_{1cy}x)}\right\} e^{j\omega t}, \tag{A.3}$$

where P_i, Q_i, R_i, S_i, and T_i are constant complex coefficients.

The time-averaged far-field energy density and the components of the time-averaged far-field intensity which take primary values as w, ϕ and ψ, can be represented as, respectively,

$$\begin{aligned}\langle e\rangle = \mathrm{Re}\Bigg[&\frac{\rho h}{4}\left(\frac{\partial w}{\partial t}\right)\left(\frac{\partial w}{\partial t}\right)^* + \frac{\rho I}{4}\left\{\left(\frac{\partial \alpha_x}{\partial t}\right)\left(\frac{\partial \alpha_x}{\partial t}\right)^* + \left(\frac{\partial \alpha_y}{\partial t}\right)\left(\frac{\partial \alpha_y}{\partial t}\right)^*\right\}\\ &+ \frac{D}{4}\left\{\left(\frac{\partial \alpha_x}{\partial x}\right)\left(\frac{\partial \alpha_x}{\partial x}\right)^* + \left(\frac{\partial \alpha_y}{\partial y}\right)\left(\frac{\partial \alpha_y}{\partial y}\right)^* + 2\nu\left(\frac{\partial \alpha_x}{\partial x}\right)\left(\frac{\partial \alpha_y}{\partial y}\right)^*\right\}\\ &+ \frac{GI}{4}\left\{\left(\frac{\partial \alpha_x}{\partial y} + \frac{\partial \alpha_y}{\partial x}\right)\left(\frac{\partial \alpha_x}{\partial y} + \frac{\partial \alpha_y}{\partial x}\right)^*\right\}\\ &+ \frac{\kappa G h}{4}\left\{\left(\frac{\partial w}{\partial x} - \alpha_x\right)\left(\frac{\partial w}{\partial x} - \alpha_x\right)^* + \left(\frac{\partial w}{\partial y} - \alpha_y\right)\left(\frac{\partial w}{\partial y} - \alpha_y\right)^*\right\}\Bigg],\end{aligned}$$

$$\begin{aligned}\langle I_x\rangle = \frac{1}{2}\mathrm{Re}\Bigg[&-D\left(\frac{\partial \alpha_x}{\partial x} + \nu\frac{\partial \alpha_y}{\partial y}\right)\left(\frac{\partial \alpha_x}{\partial t}\right)^* - (1-\nu)\frac{D}{2}\left(\frac{\partial \alpha_x}{\partial y} + \frac{\partial \alpha_y}{\partial x}\right)\left(\frac{\partial \alpha_y}{\partial t}\right)^*\\ &- \kappa G h\left(\frac{\partial w}{\partial x} - \alpha_x\right)\left(\frac{\partial w}{\partial t}\right)^*\Bigg]\end{aligned}$$

and

$$\langle I_y\rangle = \frac{1}{2}\mathrm{Re}\left[-D\left(\frac{\partial\alpha_y}{\partial y}+\nu\frac{\partial\alpha_x}{\partial x}\right)\left(\frac{\partial\alpha_y}{\partial t}\right)^* - (1-\nu)\frac{D}{2}\left(\frac{\partial\alpha_x}{\partial y}+\frac{\partial\alpha_y}{\partial x}\right)\left(\frac{\partial\alpha_x}{\partial t}\right)^* - \kappa Gh\left(\frac{\partial w}{\partial y}-\alpha_y\right)\left(\frac{\partial w}{\partial t}\right)^*\right], \quad \text{(A.4) – (A.6)}$$

where

$$\left(\frac{\partial\alpha_x}{\partial t}\right)\left(\frac{\partial\alpha_x}{\partial t}\right)^* = \left(\frac{\partial^2\phi}{\partial x\partial t}\right)\left(\frac{\partial^2\phi}{\partial x\partial t}\right)^* + \left(\frac{\partial^2\phi}{\partial x\partial t}\right)\left(\frac{\partial^2\psi}{\partial y\partial t}\right)^* + \left(\frac{\partial^2\psi}{\partial y\partial t}\right)\left(\frac{\partial^2\phi}{\partial x\partial t}\right)^* + \left(\frac{\partial^2\psi}{\partial y\partial t}\right)\left(\frac{\partial^2\psi}{\partial y\partial t}\right)^*,$$

$$\left(\frac{\partial\alpha_y}{\partial t}\right)\left(\frac{\partial\alpha_y}{\partial t}\right)^* = \left(\frac{\partial^2\phi}{\partial y\partial t}\right)\left(\frac{\partial^2\phi}{\partial y\partial t}\right)^* - \left(\frac{\partial^2\phi}{\partial y\partial t}\right)\left(\frac{\partial^2\psi}{\partial x\partial t}\right)^* - \left(\frac{\partial^2\psi}{\partial x\partial t}\right)\left(\frac{\partial^2\phi}{\partial y\partial t}\right)^* + \left(\frac{\partial^2\psi}{\partial x\partial t}\right)\left(\frac{\partial^2\psi}{\partial x\partial t}\right)^*,$$

$$\left(\frac{\partial\alpha_x}{\partial x}\right)\left(\frac{\partial\alpha_x}{\partial x}\right)^* = \left(\frac{\partial^2\phi}{\partial x^2}\right)\left(\frac{\partial^2\phi}{\partial x^2}\right)^* + \left(\frac{\partial^2\phi}{\partial x^2}\right)\left(\frac{\partial^2\psi}{\partial x\partial y}\right)^* + \left(\frac{\partial^2\psi}{\partial x\partial y}\right)\left(\frac{\partial^2\phi}{\partial x^2}\right)^* + \left(\frac{\partial^2\psi}{\partial x\partial y}\right)\left(\frac{\partial^2\psi}{\partial x\partial y}\right)^*,$$

$$\left(\frac{\partial\alpha_y}{\partial y}\right)\left(\frac{\partial\alpha_y}{\partial y}\right)^* = \left(\frac{\partial^2\phi}{\partial y^2}\right)\left(\frac{\partial^2\phi}{\partial y^2}\right)^* - \left(\frac{\partial^2\phi}{\partial y^2}\right)\left(\frac{\partial^2\psi}{\partial x\partial y}\right)^* - \left(\frac{\partial^2\psi}{\partial x\partial y}\right)\left(\frac{\partial^2\phi}{\partial y^2}\right)^* + \left(\frac{\partial^2\psi}{\partial x\partial y}\right)\left(\frac{\partial^2\psi}{\partial x\partial y}\right)^*,$$

$$\left(\frac{\partial\alpha_x}{\partial x}\right)\left(\frac{\partial\alpha_y}{\partial y}\right)^* = \left(\frac{\partial^2\phi}{\partial x^2}\right)\left(\frac{\partial^2\phi}{\partial y^2}\right)^* - \left(\frac{\partial^2\phi}{\partial x^2}\right)\left(\frac{\partial^2\psi}{\partial x\partial y}\right)^* + \left(\frac{\partial^2\psi}{\partial x\partial y}\right)\left(\frac{\partial^2\phi}{\partial y^2}\right)^* - \left(\frac{\partial^2\psi}{\partial x\partial y}\right)\left(\frac{\partial^2\psi}{\partial x\partial y}\right)^*,$$

$$\begin{aligned}\left(\frac{\partial\alpha_x}{\partial y}+\frac{\partial\alpha_y}{\partial x}\right)\left(\frac{\partial\alpha_x}{\partial y}+\frac{\partial\alpha_y}{\partial x}\right)^* &= 2\left(\frac{\partial^2\phi}{\partial x\partial y}\right)\left\{\left(\frac{\partial^2\psi}{\partial y^2}\right)^* - \left(\frac{\partial^2\psi}{\partial x^2}\right)^*\right\} + 2\left\{\left(\frac{\partial^2\psi}{\partial y^2}\right) - \left(\frac{\partial^2\psi}{\partial x^2}\right)\right\}\left(\frac{\partial^2\phi}{\partial x\partial y}\right)^* \\ &\quad + 4\left(\frac{\partial^2\phi}{\partial x\partial y}\right)\left(\frac{\partial^2\phi}{\partial x\partial y}\right)^* + \left(\frac{\partial^2\psi}{\partial x^2}\right)\left(\frac{\partial^2\psi}{\partial x^2}\right)^* + \left(\frac{\partial^2\psi}{\partial y^2}\right)\left(\frac{\partial^2\psi}{\partial y^2}\right)^* \\ &\quad - \left(\frac{\partial^2\psi}{\partial y^2}\right)\left(\frac{\partial^2\psi}{\partial x^2}\right)^* - \left(\frac{\partial^2\psi}{\partial x^2}\right)\left(\frac{\partial^2\psi}{\partial y^2}\right)^*,\end{aligned}$$

$$\begin{aligned}\left(\frac{\partial w}{\partial x}-\alpha_x\right)\left(\frac{\partial w}{\partial x}-\alpha_x\right)^* &= \left(\frac{\partial w}{\partial x}-\frac{\partial\phi}{\partial x}\right)\left(\frac{\partial w}{\partial x}-\frac{\partial\phi}{\partial x}\right)^* - \left(\frac{\partial w}{\partial x}-\frac{\partial\phi}{\partial x}\right)\left(\frac{\partial\psi}{\partial y}\right)^* \\ &\quad - \left(\frac{\partial\psi}{\partial y}\right)\left(\frac{\partial w}{\partial x}-\frac{\partial\phi}{\partial x}\right)^* + \left(\frac{\partial\psi}{\partial y}\right)\left(\frac{\partial\psi}{\partial y}\right)^*,\end{aligned}$$

$$\begin{aligned}\left(\frac{\partial w}{\partial y}-\alpha_y\right)\left(\frac{\partial w}{\partial y}-\alpha_y\right)^* &= \left(\frac{\partial w}{\partial y}-\frac{\partial\phi}{\partial y}\right)\left(\frac{\partial w}{\partial y}-\frac{\partial\phi}{\partial y}\right)^* + \left(\frac{\partial w}{\partial y}-\frac{\partial\phi}{\partial y}\right)\left(\frac{\partial\psi}{\partial x}\right)^* \\ &\quad + \left(\frac{\partial\psi}{\partial y}\right)\left(\frac{\partial w}{\partial y}-\frac{\partial\phi}{\partial y}\right)^* + \left(\frac{\partial\psi}{\partial x}\right)\left(\frac{\partial\psi}{\partial x}\right)^*,\end{aligned}$$

$$\left(\frac{\partial\alpha_x}{\partial x}\right)\left(\frac{\partial\alpha_x}{\partial t}\right)^* = \left(\frac{\partial^2\phi}{\partial x^2}\right)\left(\frac{\partial^2\phi}{\partial x\partial t}\right)^* + \left(\frac{\partial^2\phi}{\partial x^2}\right)\left(\frac{\partial^2\psi}{\partial y\partial t}\right)^* + \left(\frac{\partial^2\psi}{\partial x\partial y}\right)\left(\frac{\partial^2\phi}{\partial x\partial t}\right)^* + \left(\frac{\partial^2\psi}{\partial x\partial y}\right)\left(\frac{\partial^2\psi}{\partial y\partial t}\right)^*,$$

$$\left(\frac{\partial\alpha_y}{\partial y}\right)\left(\frac{\partial\alpha_x}{\partial t}\right)^* = \left(\frac{\partial^2\phi}{\partial y^2}\right)\left(\frac{\partial^2\phi}{\partial x\partial t}\right)^* + \left(\frac{\partial^2\phi}{\partial y^2}\right)\left(\frac{\partial^2\psi}{\partial y\partial t}\right)^* - \left(\frac{\partial^2\psi}{\partial x\partial y}\right)\left(\frac{\partial^2\phi}{\partial x\partial t}\right)^* - \left(\frac{\partial^2\psi}{\partial x\partial y}\right)\left(\frac{\partial^2\psi}{\partial y\partial t}\right)^*,$$

$$\left(\frac{\partial\alpha_x}{\partial y}+\frac{\partial\alpha_y}{\partial x}\right)\left(\frac{\partial\alpha_y}{\partial t}\right)=\left(\frac{\partial^2\phi}{\partial x\partial y}\right)\left(\frac{\partial^2\phi}{\partial y\partial t}\right)^*-\left(\frac{\partial^2\phi}{\partial x\partial y}\right)\left(\frac{\partial^2\psi}{\partial x\partial t}\right)^*+\left(\frac{\partial^2\psi}{\partial y^2}\right)\left(\frac{\partial^2\phi}{\partial y\partial t}\right)^*-\left(\frac{\partial^2\psi}{\partial y^2}\right)\left(\frac{\partial^2\psi}{\partial x\partial t}\right)^*$$
$$+\left(\frac{\partial^2\phi}{\partial x\partial y}\right)\left(\frac{\partial^2\phi}{\partial y\partial t}\right)^*-\left(\frac{\partial^2\phi}{\partial x\partial y}\right)\left(\frac{\partial^2\psi}{\partial x\partial t}\right)^*-\left(\frac{\partial^2\psi}{\partial x^2}\right)\left(\frac{\partial^2\phi}{\partial y\partial t}\right)^*+\left(\frac{\partial^2\psi}{\partial x^2}\right)\left(\frac{\partial^2\psi}{\partial x\partial t}\right)^*,$$

$$\left(\frac{\partial w}{\partial x}-\alpha_x\right)\left(\frac{\partial w}{\partial t}\right)^*=\left(\frac{\partial w}{\partial x}-\frac{\partial\phi}{\partial x}\right)\left(\frac{\partial w}{\partial t}\right)^*-\left(\frac{\partial\psi}{\partial y}\right)\left(\frac{\partial w}{\partial t}\right)^*,$$

$$\left(\frac{\partial\alpha_y}{\partial y}\right)\left(\frac{\partial\alpha_y}{\partial t}\right)^*=\left(\frac{\partial^2\phi}{\partial y^2}\right)\left(\frac{\partial^2\phi}{\partial y\partial t}\right)^*-\left(\frac{\partial^2\phi}{\partial y^2}\right)\left(\frac{\partial^2\psi}{\partial x\partial t}\right)^*-\left(\frac{\partial^2\psi}{\partial x\partial y}\right)\left(\frac{\partial^2\phi}{\partial y\partial t}\right)^*+\left(\frac{\partial^2\psi}{\partial x\partial y}\right)\left(\frac{\partial^2\psi}{\partial x\partial t}\right)^*,$$

$$\left(\frac{\partial\alpha_x}{\partial x}\right)\left(\frac{\partial\alpha_y}{\partial t}\right)^*=\left(\frac{\partial^2\phi}{\partial x^2}\right)\left(\frac{\partial^2\phi}{\partial y\partial t}\right)^*-\left(\frac{\partial^2\phi}{\partial x^2}\right)\left(\frac{\partial^2\psi}{\partial x\partial t}\right)^*+\left(\frac{\partial^2\psi}{\partial x\partial y}\right)\left(\frac{\partial^2\phi}{\partial y\partial t}\right)^*-\left(\frac{\partial^2\psi}{\partial x\partial y}\right)\left(\frac{\partial^2\psi}{\partial x\partial t}\right)^*,$$

$$\left(\frac{\partial\alpha_x}{\partial y}+\frac{\partial\alpha_y}{\partial x}\right)\left(\frac{\partial\alpha_x}{\partial t}\right)^*=\left(\frac{\partial^2\phi}{\partial x\partial y}\right)\left(\frac{\partial^2\phi}{\partial x\partial t}\right)^*+\left(\frac{\partial^2\phi}{\partial x\partial y}\right)\left(\frac{\partial^2\psi}{\partial y\partial t}\right)^*+\left(\frac{\partial^2\psi}{\partial y^2}\right)\left(\frac{\partial^2\phi}{\partial x\partial t}\right)^*+\left(\frac{\partial^2\psi}{\partial y^2}\right)\left(\frac{\partial^2\psi}{\partial y\partial t}\right)^*$$
$$+\left(\frac{\partial^2\phi}{\partial x\partial y}\right)\left(\frac{\partial^2\phi}{\partial x\partial t}\right)^*+\left(\frac{\partial^2\phi}{\partial x\partial y}\right)\left(\frac{\partial^2\psi}{\partial y\partial t}\right)^*-\left(\frac{\partial^2\psi}{\partial x^2}\right)\left(\frac{\partial^2\phi}{\partial x\partial t}\right)^*+\left(\frac{\partial^2\psi}{\partial x^2}\right)\left(\frac{\partial^2\psi}{\partial y\partial t}\right)^*$$

and

$$\left(\frac{\partial w}{\partial y}-\alpha_y\right)\left(\frac{\partial w}{\partial t}\right)^*=\left(\frac{\partial w}{\partial y}-\frac{\partial\phi}{\partial y}\right)\left(\frac{\partial w}{\partial t}\right)^*+\left(\frac{\partial\psi}{\partial x}\right)\left(\frac{\partial w}{\partial t}\right)^*. \quad \text{(A.7)}-\text{(A.22)}$$

The time-averaged far-field energy density and intensity can be obtained by substituting Eqs. (A.1)–(A.3) into Eqs. (A.4), and (A.5) and (A.6), respectively. However, the obvious relation between the time-averaged far-field energy density and power which are obtained by this means are not found. Therefore, to eliminate terms that are spatially harmonic in the time-averaged far-field energy density and intensity, the locally space averaged value is obtained as follows:

$$\langle\bar{e}\rangle=\frac{k_{i1x}k_{i1y}}{\pi^2}\int_0^{\pi/k_{i1y}}\int_0^{\pi/k_{i1x}}\langle e\rangle\,\mathrm{d}x\,\mathrm{d}y\quad(i=1,2,3) \tag{A.23}$$

and

$$\langle\bar{\mathrm{I}}\rangle=\frac{k_{i1x}k_{i1y}}{\pi^2}\int_0^{\pi/k_{i1y}}\int_0^{\pi/k_{i1x}}\langle\vec{I}\rangle\,\mathrm{d}x\,\mathrm{d}y\quad(i=1,2,3), \tag{A.24}$$

where $\langle\bar{e}\rangle$ and $\langle\bar{\mathrm{I}}\rangle$ are the time- and locally space-averaged far-field smooth energy density and intensity, respectively, and $\langle\bar{\mathrm{I}}\rangle=\langle\bar{I}_x\rangle\vec{i}+\langle\bar{I}_y\rangle\vec{j}$. For instance, Eq. (A.7) in the time-averaged far-field energy density is represented as

$$\left(\frac{\partial\alpha_x}{\partial t}\right)\left(\frac{\partial\alpha_x}{\partial t}\right)^*=\omega^2|k_{2cx}|^2(|[R_1]^{--}|^2+|[R_2]^{-+}|^2+|[R_3]^{+-}|^2+|[R_4]^{++}|^2)$$
$$+\omega^2|k_{3cx}|^2(|[S_1]^{--}|^2+|[S_2]^{-+}|^2+|[S_3]^{+-}|^2+|[S_4]^{++}|^2)$$
$$+\omega^2|k_{2cx}|^2\{[R_1]^{--}([R_2]^{-+}-[R_3]^{+-}-[R_4]^{++})^*+[R_2]^{-+}([R_1]^{--}-[R_3]^{+-}-[R_4]^{++})^*$$
$$-[R_3]^{+-}([R_1]^{--}+[R_2]^{-+}-[R_4]^{++})^*-[R_4]^{++}([R_1]^{--}+[R_2]^{-+}-[R_3]^{+-})^*\}$$
$$+\omega^2|k_{3cx}|^2\{[S_1]^{--}([S_2]^{-+}-[S_3]^{+-}-[S_4]^{++})^*+[S_2]^{-+}([S_1]^{--}-[S_3]^{+-}-[S_4]^{++})^*$$
$$-[S_3]^{+-}([S_1]^{--}+[S_2]^{-+}-[S_4]^{++})^*-[S_4]^{++}([S_1]^{--}+[S_2]^{-+}-[S_3]^{+-})^*\}$$
$$+\omega^2(k_{2cx}k_{3cx}^*)([R_1]^{--}+[R_2]^{-+}-[R_3]^{+-}-[R_4]^{++})([S_1]^{--}+[S_2]^{-+}-[S_3]^{+-}-[S_4]^{++})^*$$

$$
\begin{aligned}
&+\omega^2(k_{3cx}k_{2cx}^*)([S_1]^{--}+[S_2]^{-+}-[S_3]^{+-}-[S_4]^{++})([R_1]^{--}+[R_2]^{-+}-[R_3]^{+-}-[R_4]^{++})^*\\
&+\{\omega k_{2cx}([R_1]^{--}+[R_2]^{-+}-[R_3]^{+-}-[R_4]^{++})+\omega k_{3cx}([S_1]^{--}+[S_2]^{-+}-[S_3]^{+-}-[S_4]^{++})\}\\
&\times\{\omega k_{1cy}([T_1]^{--}-[T_2]^{-+}+[T_3]^{+-}-[T_4]^{++})\}^*+\{\omega k_{1cy}([T_1]^{--}-[T_2]^{-+}+[T_3]^{+-}-[T_4]^{++})\}\\
&\times\{\omega k_{2cx}([R_1]^{--}+[R_2]^{-+}-[R_3]^{+-}-[R_4]^{++})+\omega k_{3cx}([S_1]^{--}+[S_2]^{-+}-[S_3]^{+-}-[S_4]^{++})\}^*\\
&+\omega^2|k_{1cy}|^2(|[T_1]^{--}|^2+|[T_2]^{-+}|^2+|[T_3]^{+-}|^2+|[T_4]^{++}|^2)\\
&+\omega k_{1cy}\{[T_1]^{--}(-[T_2]^{-+}+[T_3]^{+-}-[T_4]^{++})^*-[T_2]^{-+}([T_1]^{--}+[T_3]^{+-}-[T_4]^{++})^*\\
&+[T_3]^{+-}([T_1]^{--}-[T_2]^{-+}-[T_4]^{++})^*-[T_4]^{++}([T_1]^{--}-[T_2]^{-+}+[T_3]^{+-})^*\}
\end{aligned}
\tag{A.25}
$$

where $[\,]^{\pm\pm}=[\,]\times\exp(\pm k_{cx}x\pm k_{cy}y)$.

In Eq. (A.25), the terms like $(|[R_1]^{--}|^2,\ldots,\ |[S_1]^{--}|^2,\ldots,\ |[T_4]^{++}|^2)$ are purely exponentially decayed components and the other terms like $([R_1]^{--}([R_2]^{-+})^*,\ldots,\ [S_4]^{++}\ ([R_4]^{++})^*,\ldots,\ [T_4]^{++}\ ([T_3]^{+-})^*)$ are spatially harmonic components. Therefore, using the local space-average to eliminate spatially harmonic terms, Eq. (A.25) is expressed by

$$
\begin{aligned}
\left[\left(\frac{\partial\alpha_x}{\partial t}\right)\left(\frac{\partial\alpha_x}{\partial t}\right)^*\right]&=\omega^2|k_{1cy}|^2(|[T_1]^{--}|^2+|[T_2]^{-+}|^2+|[T_3]^{+-}|^2+|[T_4]^{++}|^2)\\
&+\omega^2|k_{2cx}|^2(|[R_1]^{--}|^2+|[R_2]^{-+}|^2+|[R_3]^{+-}|^2+|[R_4]^{++}|^2)\\
&+\omega^2|k_{3cx}|^2(|[S_1]^{--}|^2+|[S_2]^{-+}|^2+|[S_3]^{+-}|^2+|[S_4]^{++}|^2).
\end{aligned}
\tag{A.26}
$$

Apply this procedure to the other terms, for small damping, the time- and locally space-averaged far-field smooth energy density and components of intensity are obtained by, respectively,

$$
\begin{aligned}
\langle\bar{e}\rangle&=\tfrac{1}{4}[(\rho I\omega^2+\kappa Gh)k_{11}^2+GIk_{11}^4]\times(|[T_1]^{--}|^2+|[T_2]^{-+}|^2+|[T_3]^{+-}|^2+|[T_4]^{++}|^2)\\
&+\tfrac{1}{4}[(\rho h\omega^2-\kappa Ghk_{21}^2)^2(Dk_{21}^4+\rho I\omega^2k_{21}^2)+k_{21}^2(\rho h\omega^2)(\kappa Gh)(\kappa Ghk_{21}^2+\rho h\omega^2)]\\
&\times(|[R_1]^{--}|^2+|[R_2]^{-+}|^2+|[R_3]^{+-}|^2+|[R_4]^{++}|^2)\\
&+\tfrac{1}{4}[(\rho h\omega^2-\kappa Ghk_{31}^2)^2(Dk_{31}^4+\rho I\omega^2k_{31}^2)+k_{31}^2(\rho h\omega^2)(\kappa Gh)(\kappa Ghk_{31}^2+\rho h\omega^2)]\\
&\times(|[S_1]^{--}|^2+|[S_2]^{-+}|^2+|[S_3]^{+-}|^2+|[S_4]^{++}|^2),
\end{aligned}
\tag{A.27}
$$

$$
\begin{aligned}
\langle\bar{I}_x\rangle&=\frac{1}{2}\left[\frac{D}{2}(1-\nu)\omega k_{11x}k_{11}^2\right]\times(|[T_1]^{--}|^2+|[T_2]^{-+}|^2-|[T_3]^{+-}|^2-|[T_4]^{++}|^2)\\
&+\frac{1}{2}[D(\rho h\omega^2-\kappa Ghk_{21}^2)^2\omega k_{21x}k_{21}^2+(\rho h\omega^2)(\omega k_{21x})(\kappa Ghk_{21})^2]\\
&\times(|[R_1]^{--}|^2+|[R_2]^{-+}|^2-|[R_3]^{+-}|^2-|[R_4]^{++}|^2)\\
&+\frac{1}{2}[D(\rho h\omega^2-\kappa Ghk_{31}^2)^2\omega k_{31x}k_{31}^2+(\rho h\omega^2)(\omega k_{31x})(\kappa Ghk_{31})^2]\\
&\times(|[S_1]^{--}|^2+|[S_2]^{-+}|^2-|[S_3]^{+-}|^2-|[S_4]^{++}|^2)
\end{aligned}
\tag{A.28}
$$

and

$$
\begin{aligned}
\langle\bar{I}_y\rangle&=\frac{1}{2}\left[\frac{D}{2}(1-\nu)\omega k_{11y}k_{11}^2\right]\times(|[T_1]^{--}|^2-|[T_2]^{-+}|^2+|[T_3]^{+-}|^2-|[T_4]^{++}|^2)\\
&+\frac{1}{2}[D(\rho h\omega^2-\kappa Ghk_{21}^2)^2\omega k_{21y}k_{21}^2+(\rho h\omega^2)(\omega k_{21y})(\kappa Ghk_{21})^2]\\
&\times(|[R_1]^{--}|^2-|[R_2]^{-+}|^2+|[R_3]^{+-}|^2-|[R_4]^{++}|^2)\\
&+\frac{1}{2}[D(\rho h\omega^2-\kappa Ghk_{31}^2)^2\omega k_{31y}k_{31}^2+(\rho h\omega^2)(\omega k_{31y})(\kappa Ghk_{31})^2]\\
&\times(|[S_1]^{--}|^2+|[S_2]^{-+}|^2-|[S_3]^{+-}|^2-|[S_4]^{++}|^2).
\end{aligned}
\tag{A.29}
$$

A.2. Below the critical frequency

Below the critical frequency, the only BDFW with wavenumber k_{2c} is a far-field solution and the OPSW, displacement potential function ψ, is a pure near-field solution. Therefore, the far-field solution composed of the transverse displacement w and displacement potential functions ϕ can be rewritten as, respectively,

$$w = \{P_1 e^{(-jk_{2cx}x - jk_{2cy}y)} + P_2 e^{(-jk_{2cx}x + jk_{2cy}y)} + P_3 e^{(jk_{2cx}x - jk_{2cy}y)} + P_4 e^{(jk_{2cx}x + jk_{2cy}y)}\} e^{j\omega t} \tag{A.30}$$

and

$$\phi = \{Q_1 e^{(-jk_{2cx}x - jk_{2cy}y)} + Q_2 e^{(-jk_{2cx}x + jk_{2cy}y)} + Q_3 e^{(jk_{2cx}x - jk_{2cy}y)} + Q_4 e^{(jk_{2cx}x + jk_{2cy}y)}\} e^{j\omega t}. \tag{A.31}$$

Substituting Eqs. (A.30) and (A.31) into Eqs. (A.4)–(A.6), the time-averaged far-field energy density and intensity of out-of-plane waves in the Mindlin plate are obtained. In this case, like the previous case, the local space-average is applied to the time-averaged far-field energy density and intensity in order to eliminate spatially harmonic terms.

The time- and locally space-averaged far-field smooth energy density and intensity are expressed by

$$\begin{aligned}\langle \bar{e} \rangle = {} & \tfrac{1}{4}[(\rho h\omega^2 - \kappa G h k_{21}^2)^2 (D k_{21}^4 + \rho I \omega^2 k_{21}^2) + k_{21}^2 (\rho h \omega^2)(\kappa G h)(\kappa G h k_{21}^2 + \rho h \omega^2)] \\ & \times (|[R_1]^{--}|^2 + |[R_2]^{-+}|^2 + |[R_3]^{+-}|^2 + |[R_4]^{++}|^2),\end{aligned} \tag{A.32}$$

$$\begin{aligned}\langle \bar{I}_x \rangle = {} & \tfrac{1}{2}[D(\rho h\omega^2 - \kappa G h k_{21}^2)^2 \omega k_{21x} k_{21}^2 + (\rho h \omega^2)(\omega k_{21x})(\kappa G h k_{21})^2] \\ & \times (|[R_1]^{--}|^2 + |[R_2]^{-+}|^2 + |[R_3]^{+-}|^2 + |[R_4]^{++}|^2)\end{aligned} \tag{A.33}$$

and

$$\begin{aligned}\langle \bar{I}_y \rangle = {} & \tfrac{1}{2}[D(\rho h\omega^2 - \kappa G h k_{21}^2)^2 \omega k_{21y} k_{21}^2 + (\rho h \omega^2)(\omega k_{21y})(\kappa G h k_{21})^2] \\ & \times (|[R_1]^{--}|^2 - |[R_2]^{-+}|^2 + |[R_3]^{+-}|^2 - |[R_4]^{++}|^2).\end{aligned} \tag{A.34}$$

Appendix B. Classical solution of out-of-plane motions in the Mindlin plate

The equations of out-of-plane motion in the Mindlin plate excited by a harmonic point force are given by

$$D\left[\frac{\partial^2 \alpha_x}{\partial x^2} + \frac{(1-\nu)}{2}\frac{\partial^2 \alpha_x}{\partial y^2} + \frac{(1+\nu)}{2}\frac{\partial^2 \alpha_y}{\partial x \partial y}\right] + \kappa G h\left(\frac{\partial w}{\partial x} - \alpha_x\right) - I\rho\frac{\partial^2 \alpha_x}{\partial t^2} = 0, \tag{B.1}$$

$$D\left[\frac{(1-\nu)}{2}\frac{\partial^2 \alpha_y}{\partial x^2} + \frac{\partial^2 \alpha_y}{\partial^2 y} + \frac{(1+\nu)}{2}\frac{\partial^2 \alpha_x}{\partial x \partial y}\right] + \kappa G h\left(\frac{\partial w}{\partial y} - \alpha_y\right) - I\rho\frac{\partial^2 \alpha_y}{\partial t^2} = 0 \tag{B.2}$$

and

$$-\kappa G h\left(\frac{\partial^2 w}{\partial x^2} + \frac{\partial^2 w}{\partial y^2} - \frac{\partial \alpha_x}{\partial x} - \frac{\partial \alpha_y}{\partial y}\right) + \rho h\frac{\partial w^2}{\partial t^2} = F\delta(x - x_0)\delta(y - y_0)e^{j\omega t}, \tag{B.3}$$

where F is the amplitude of external point force and (x_0, y_0) is the excitation position.

When the plate is simply supported along its edges, the transverse displacement w, and the angles of rotation due to bending α_x and α_y can be expressed by using the double trigonometric series of the spatial variables x and y, respectively,

$$w(x, y, t) = \sum_{m=0}^{\infty}\sum_{n=0}^{\infty} A_{mn} \sin\left(\frac{m\pi x}{L_x}\right)\sin\left(\frac{n\pi y}{L_y}\right)e^{j\omega t}, \tag{B.4}$$

$$\alpha_x(x, y, t) = \sum_{m=0}^{\infty}\sum_{n=0}^{\infty} B_{mn} \cos\left(\frac{m\pi x}{L_x}\right)\sin\left(\frac{n\pi y}{L_y}\right)e^{j\omega t} \tag{B.5}$$

and

$$\alpha_y(x,y,t)=\sum_{m=0}^{\infty}\sum_{n=0}^{\infty}C_{mn}\sin\left(\frac{m\pi x}{L_x}\right)\cos\left(\frac{n\pi y}{L_y}\right)e^{j\omega t}, \tag{B.6}$$

where A_{mn}, B_{mn} and C_{mn} are modal participation factors of variables.

Using the double series of the sine function, the external force is also expressed by,

$$F\delta(x-x_0)\delta(y-y_0)e^{j\omega t}=\sum_{m=0}^{\infty}\sum_{n=0}^{\infty}F_{mn}\sin\left(\frac{m\pi x}{L_x}\right)\sin\left(\frac{n\pi y}{L_y}\right)e^{j\omega t}. \tag{B.7}$$

By the orthogonality of sine functions in Eq. (B.7), the modal force factor F_{mn} is obtained by

$$F_{mn}=\frac{4F}{L_xL_y}\sin\left(\frac{m\pi x_0}{L_x}\right)\sin\left(\frac{n\pi y_0}{L_y}\right). \tag{B.8}$$

Substituting Eqs. (B.4)–(B.6) into Eqs. (B.1)–(B.3), the following matrix equation is obtained:

$$\begin{bmatrix}\varepsilon_{11}&\varepsilon_{12}&\varepsilon_{13}\\ \varepsilon_{21}&\varepsilon_{22}&\varepsilon_{23}\\ \varepsilon_{31}&\varepsilon_{32}&\varepsilon_{33}\end{bmatrix}\begin{Bmatrix}A_{mn}\\ B_{mn}\\ C_{mn}\end{Bmatrix}=\begin{Bmatrix}0\\ 0\\ F_{mn}\end{Bmatrix}, \tag{B.9}$$

where

$$\begin{aligned}
\varepsilon_{11}&=\kappa G_c h(m\pi/L_x),\\
\varepsilon_{12}&=-D_c\{(m\pi/L_x)^2+(n\pi/L_y)^2(1-\nu)/2\}+\rho I\omega^2-\kappa G_c h,\\
\varepsilon_{13}&=-D_c(m\pi/L_x)(n\pi/L_y)(1+\nu)/2,\\
\varepsilon_{21}&=\kappa G_c h(n\pi/L_y),\\
\varepsilon_{22}&=-D_c(m\pi/L_x)(n\pi/L_y)(1+\nu)/2,\\
\varepsilon_{23}&=-D_c\{(m\pi/L_x)^2(1-\nu)/2+(n\pi/L_y)^2\}+\rho I\omega^2-\kappa G_c h,\\
\varepsilon_{31}&=\kappa G_c h\{(m\pi/L_x)^2+(n\pi/L_y)^2\}-\rho h\omega^2,\\
\varepsilon_{32}&=-\kappa G_c h(m\pi/L_x)\\
&\text{and}\\
\varepsilon_{33}&=-\kappa G_c h(n\pi/L_y).
\end{aligned}$$

By Eq. (B.9), the transverse displacement w and the angles of rotation due to bending α_x and α_y can be rewritten as, using only the modal participation factor A_{mn},

$$w(x,y,t)=\sum_{m=0}^{\infty}\sum_{n=0}^{\infty}A_{mn}\sin\left(\frac{m\pi x}{L_x}\right)\sin\left(\frac{n\pi y}{L_y}\right)e^{j\omega t}, \tag{B.10}$$

$$\alpha_x(x,y,t)=\sum_{m=0}^{\infty}\sum_{n=0}^{\infty}\left\{A_{mn}\frac{(\varepsilon_{13}\varepsilon_{21}-\varepsilon_{23}\varepsilon_{11})}{(\varepsilon_{12}\varepsilon_{23}-\varepsilon_{13}\varepsilon_{22})}\right\}\cos\left(\frac{m\pi x}{L_x}\right)\sin\left(\frac{n\pi y}{L_y}\right)e^{j\omega t} \tag{B.11}$$

and

$$\alpha_y(x,y,t)=\sum_{m=0}^{\infty}\sum_{n=0}^{\infty}\left\{A_{mn}\frac{(\varepsilon_{22}\varepsilon_{11}-\varepsilon_{12}\varepsilon_{21})}{(\varepsilon_{12}\varepsilon_{23}-\varepsilon_{13}\varepsilon_{22})}\right\}\sin\left(\frac{m\pi x}{L_x}\right)\cos\left(\frac{n\pi y}{L_y}\right)e^{j\omega t}, \tag{B.12}$$

where

$$A_{mn} = \frac{\dfrac{4F}{L_x L_y}\sin\left(\dfrac{m\pi x_0}{L_x}\right)\sin\left(\dfrac{n\pi y_0}{L_y}\right)}{\left[\kappa G_c h\left\{\left(\dfrac{m\pi}{L_x}\right)^2+\left(\dfrac{n\pi}{L_y}\right)^2-\left(\dfrac{m\pi}{L_x}\right)\dfrac{(\varepsilon_{13}\varepsilon_{21}-\varepsilon_{23}\varepsilon_{11})}{(\varepsilon_{12}\varepsilon_{23}-\varepsilon_{13}\varepsilon_{22})}-\left(\dfrac{n\pi}{L_y}\right)\dfrac{(\varepsilon_{22}\varepsilon_{11}-\varepsilon_{12}\varepsilon_{21})}{(\varepsilon_{12}\varepsilon_{23}-\varepsilon_{13}\varepsilon_{22})}\right\}-\rho h\omega^2\right]}. \quad \text{(B.13)}$$

References

[1] B.D. Seckler, J.B. Keller, Geometrical theory of diffraction in inhomogeneous media, *Journal of the Acoustical Society of America* 31 (2) (1959) 192–205.

[2] J.B. Keller, *Wave Propagation and Underwater Acoustics, Lecture Notes Physics*, Vol. 70, Springer, New York, 1977.

[3] Paul Filippi, Dominique Habault, J.P. Lefebvre, A. Bergassoli, *Acoustics: Basic Physics, Theory and Methods*, Academic Press, New York, 1999.

[4] L.J. Fradkin, A.P. Kiselev, The two-component representation of time-harmonic elastic body waves in the high- and intermediate-frequency regimes, *Journal of the Acoustical Society of America* 101 (1) (1997) 52–65.

[5] R. Gunda, S.M. Vijayakar, R. Singh, Method of images for the harmonic response of beams and rectangular plates, *Journal of Sound and Vibration* 185 (1995) 791–808.

[6] F.J. Fahy, Statistical energy analysis and vibrational power flow, *Third International Congress on Intensity Techniques*, Senlis France, 1990, pp. 29–34.

[7] L. Cremer, M. Heckl, *Structure-Borne Sound: structural vibrations and sound radiation at audio frequencies*, second ed., Springer, Berlin, 1988.

[8] L.A. Wood, C.A. Joachim, Interior noise scatter in four-cylinder sedans and wagons, *International Journal of Vehicle Design* 8 (4/5/6) (1987) 428–438.

[9] M.S. Kompella, R.J. Bernhard, Measurement of the statistical variation of structural-acoustic characteristics of automotive vehicles, *SAE Noise & Vibration Conference*, Traverse City, Michigan, USA, 1993.

[10] R.H. Lyon, R.G. Dejong, *Theory and Application of Statistical Energy Analysis*, second ed., Butterworth-Heinemann, London, 1995.

[11] R.H. Lyon, E. Eichler, Random vibration of connected structures, *Journal of the Acoustical Society of America* 36 (1964) 1344–1354.

[12] R.H. Lyon, Statistical analysis of power injection and response in structures and rooms, *Journal of the Acoustical Society of America* 38 (1965) 545–565.

[13] P.E. Cho, Energy Flow Analysis of Coupled Structures, Ph.D. Dissertation, Purdue University, 1993.

[14] V.D. Belov, S.A. Rybak, B.D. Tartakovskii, Propagation of vibrational energy in absorbing structures, *Journal of Soviet Physics Acoustics* 23 (2) (1977) 115–119.

[15] D.J. Nefske, S.H. Sung, Power flow finite element analysis of dynamic systems: basic theory and application to beams, *Journal of Vibration, Acoustics, Stress and Reliability in Design* 111 (1989) 94–100.

[16] J. Wohlever, Vibrational Power Flow Analysis of Rods and Beams, Master Thesis, Purdue University, 1989.

[17] J.C. Wohlever, R.J. Bernhard, Mechanical energy flow models of rods and beams, *Journal of Sound and Vibration* 153 (1) (1992) 1–19.

[18] O.M. Bouthier, The Energetics of Plates, Ph.D. Dissertation, Purdue University, 1992.

[19] O.M. Bouthier, R.J. Bernhard, Models of space-averaged energetics of plates, *American Institute of Aeronautics and Astronautics Journal* 30 (3) (1992) 616–623.

[20] O.M. Bouthier, R.J. Bernhard, Simple models of the energetics of transversely vibrating plates, *Journal of Sound and Vibration* 182 (1) (1995) 149–164.

[21] O.M. Bouthier, R.J. Bernhard, C. Wohlever, Energy and structural intensity formulations of beam and plate vibrations, *Proceedings of the 3rd International Congress on Intensity Techniques*, Senlis, France, 1999, pp. 37–44.

[22] D.-H. Park, S.-Y. Hong, H.-G. Kil, J.-J. Jeon, Power flow models and analysis of in-plane waves in finite coupled thin plates, *Journal of Sound and Vibration* 244 (4) (2001) 651–668.

[23] R.S. Langley, Analysis of beam and plate vibrations by using the wave equation, *Journal of Sound and Vibration* 150 (1991) 47–65.

[24] R.S. Langley, On the vibrational conductivity approach to high frequency dynamics for two-dimensional structural components, *Journal of Sound and Vibration* 182 (1995) 637–657.

[25] H.S. Kim, H.J. Kang, J.S. Kim, A vibrational analysis at high frequencies by the power flow method, *Journal of Sound and Vibration* 174 (1994) 493–504.

[26] M.J. Smith, A hybrid energy method for predicting high frequency vibrational response of point-loaded plates, *Journal of Sound and Vibration* 202 (1995) 375–394.

[27] A. Le Bot, A vibroacustic model for high frequency analysis, *Journal of Sound and Vibration* 211 (1998) 537–554.

[28] A. Le Bot, Geometric diffusion of vibrational energy and comparison with the vibrational conductivity approach, *Journal of Sound and Vibration* 212 (1998) 637–647.

[29] Y. Lase, L. Jezequel, Analysis of a dynamic system based on a new energetics formulation, *Paper presented at Third International Congress on Intensity Techniques*, Senlis, France, 1990, pp. 145–150.

[30] Y. Lase, M.N. Ichchou, L. Jezequel, Energy flow analysis of bars and beams: theoretical formulations, *Journal of Sound and Vibration* 192 (1) (1996) 281–305.
[31] Y.-H. Park, S.-Y. Hong, Vibrational energy flow analysis of corrected flexural waves in Timoshenko Beam—Part I: Theory of an energetic model, *Shock and Vibration* 13 (2006) 137–165.
[32] Y.-H. Park, S.-Y. Hong, Vibrational energy flow analysis of corrected flexural waves in Timoshenko beam—Park II: Application to coupled Timoshenko beams, *Shock and Vibration* 13 (2006) 167–196.
[33] K.M. Liew, Y. Xiang, S. Kitipornchai, Research on thick plate vibration: a literature survey, *Journal of Sound and Vibration* 180 (1) (1995) 163–176.
[34] W. Soedel, *Vibrations of Shells and Plates*, second ed., Dekker, New York, 1993.
[35] H.M. Nelson, High frequency flexural vibration of thick rectangular bars and plates, *Journal of Sound and Vibration* 60 (1) (1978) 101–118.
[36] D.U. Noiseux, Measurement of power flow in uniform beams and plates, *Journal of the Acoustical Society of America* 47 (1) (1970) 238–247.
[37] L.E. Kinsler, A.R. Frey, A.B. Coppens, J.V. Sanders, *Fundamentals of Acoustics*, Wiley, New York, 1982.